PREDICTING BENDING BEHAVIOUR OF DEPLOYABLE BOOMS MADE OF THIN WOVEN FIBRE COMPOSITES

D.C.D.K. Karannagodage

178085P

Degree of Master of Science

Department of Civil Engineering

University of Moratuwa

Sri Lanka

December 2018

PREDICTING BENDING BEHAVIOUR OF DEPLOYABLE BOOMS MADE OF THIN WOVEN FIBRE COMPOSITES

D.C.D.K. Karannagodage

178085P

Thesis submitted in partial fulfilment of the requirements for the degree Master of Science in Civil Engineering

Department of Civil Engineering

University of Moratuwa

Sri Lanka

December 2018

Declaration

I declare that this is my own work and this thesis does not incorporate without acknowledgement any material previously submitted for a Degree or Diploma in any other University or institute of higher learning and to the best of my knowledge and belief it does not contain any material previously published or written by another person except where the acknowledgement is made in the text.

Also, I hereby grant to University of Moratuwa the non-exclusive right to reproduce and distribute my thesis, in whole or in part in print, electronic or other medium. I retain the right to use this content in whole or part in future works (such as articles or books).

…… Date: 1st December 2018

D.C.D.K. Karannagodage

The above candidate has carried out research for the Masters under my supervision.

…… Date: 1st December 2018

Dr. H.M.Y.C. Mallikarachchi

Abstract

Design of advanced space structures like solar sails and reflectors are limited by the volume and payload capacity of launch vehicles. Thus, there is a trend to utilize deployable structures made of ultra-thin fibre composite materials over traditional mechanical hinges. Use of thin woven fibre composites enables them to self-deploy using stored strain energy and hence unfolds several benefits such as high strength to weight ratio, less complexity, negligible frictional effects during deployment.

Booms made of thin fibre composite with epoxy matrix have been widely used in space structures since 1980s. Even though the deformable booms with ultra-thin composites conquer the aforementioned limitations, folding of such structures are limited to their elastic regime. Once the folding is extended beyond the elastic region, these composites are either subjected to fibre failure or to plastic deformation of matrix. Thus, now scientists are investigating the possibility of using more flexible elastomers, i.e. silicone which allows the fibres to micro-buckle and hence survive under extreme curvatures.

However, use of soft elastomers in space structures can lead to poor structural performance after deployment. Also the composites like Carbon Fibre Reinforced Silicone (CFRS) are unable to store enough strain energy to provide required force for self-deployment when released.

Dual matrix fibre composites were invented to solve that problem. Dual matrix fibre composites contain a continuous fibre reinforcement with soft elastomeric matrix like silicon in specified hinge regions and traditional epoxy matrix elsewhere to stabilize the deploying behaviour. Thus, the dual-matrix composites can entertain the high curvatures up to 180^0 without failures in the deployable structures. As this matrix medium allows the fibres to micro-buckle (stress relief mechanism for the fibres in the compression zone) that enhance the folding mechanism to achieve higher curvatures without showing significant damage to the fibres in nonlinear region.

It has been observed that these woven fibre-silicone composites have a highly non-linear moment-curvature relationship while there is no significant variation in

axial stiffness. Further it has been shown that the classical lamination theory is over predicting the bending stiffness by 2 – 4 times when it comes to woven composites made of one to three plies.

This research is focussed on understanding the influence of varying bending stiffness with the degree of deformation in predicting quasi-static deployment behaviour of dual-matrix composite booms. A case-study of a three-ply dual-matrix composite boom made of thin woven glass fibre has been selected and simulated with a commercial finite element package. It has been shown that bending stiffness of the soft-elastomer region needs to be varied with the degree of deformation for accurate predictions.

Change of bending stiffness is attempted in three different methods. First the analysis has been performed with a series of independent simulations with specified bending stiffness for each model. Secondly the possibility of using import analysis where stress and material state is imported from a previous step. Finally an attempt is made to develop user-subroutine where the bending stiffness properties of the structure can be concurrently updated with degree of deformation.

Key Words: deployable booms, dual-matrix composites, moment-rotation response, user-subroutine

Dedication

To my beloved parents and sister, without whom none of my success would be possible.

Acknowledgement

First of all I would like to express my sincere gratitude to my research supervisor and mentor Dr. Chinthaka Mallikarachchi for his technical guidance and encouragement throughout the research. I would also like to thank Prof. Priyan Dias and Prof. Rangika Halwatura for providing valuable comments and advices during progress reviews.

My special thanks goes to the academic staff of Civil Engineering Department, University of Moratuwa. I am grateful to Seyon Mierunalan, Varakini Sanmugadas, Milinda Yapa, Kanthasamy Ubamanyu, Hasitha Wijesuriya and Sahangi Dassanayake for helpful discussions and immense support given as research colleagues throughout this research.

Finally, I want to thank the Senate Research Committee of University of Moratuwa, National Research Council, Sri Lanka and Ceylon Steel Cooperation for providing financial support.

Table of Contents

List of Figures

List of Tables

Nomenclature

List of Abbreviations

DNSC	Danish National Space Centre
NASA	National Aeronautics and Space Administration
CFRS	Carbon Fibre Reinforced Silicone
FRC	Fibre-Reinforce Composites
CLT	Classical Lamination Theory
CFRS	Carbon Fibre Reinforced Silicone
UD	Unidirectional

List of Symbols

$\bar{Q}$	Ply stiffness
M	Deployment moment
θ	Rotational angle
ABD_E	Constitutive relationship of AQ/Epoxy
ABD_S	Constitutive relationship of AQ/Silicon
$\propto$	Time scaling factor
ξ	Fraction of critical damping in the fundamental frequency mode
l_{min}	Shortest length of finite element
c_d	Dilatation wave speed
E	Modulus of elasticity
P	Material density
$\dot{\epsilon}_{vol}$	Volumetric strain
c_v	Damping coefficient

v	Velocity
n	Normal vector
v	Poisson's ratio
E_{tot}	Total energy stored and/or dissipated
E_{wk}	Work of external forces
E_i	Summation of internal energy
E_{vd}	Viscous dissipation
E_{ke}	Kinetic energy

CHAPTER I

1. Background

Increased range and power requirements in space exploration require structures with a larger surface area, like solar sails, reflectors and sunshields. Limited space available on launch vehicles has become the main bottleneck in designing such applications. Hence the concept of deployable structures, where a larger structure can be folded into a compact configuration during transportation, is at supreme interest at present [1], [2].

1.1. Self-Deployable Structures

Use of rigid assemblies with mechanical hinges that are associated with motors and springs for actuation lead to higher weight and increased complexity. Elastically deformable thin fibre composites that are capable of deploying with stored energy has been introduced in deployable structures as a feasible alternative for these weight sensitive applications [3], [4]. Some examples for these wide range of applications are solar sails, solar panels. antennae and booms (see Figure 1.1).

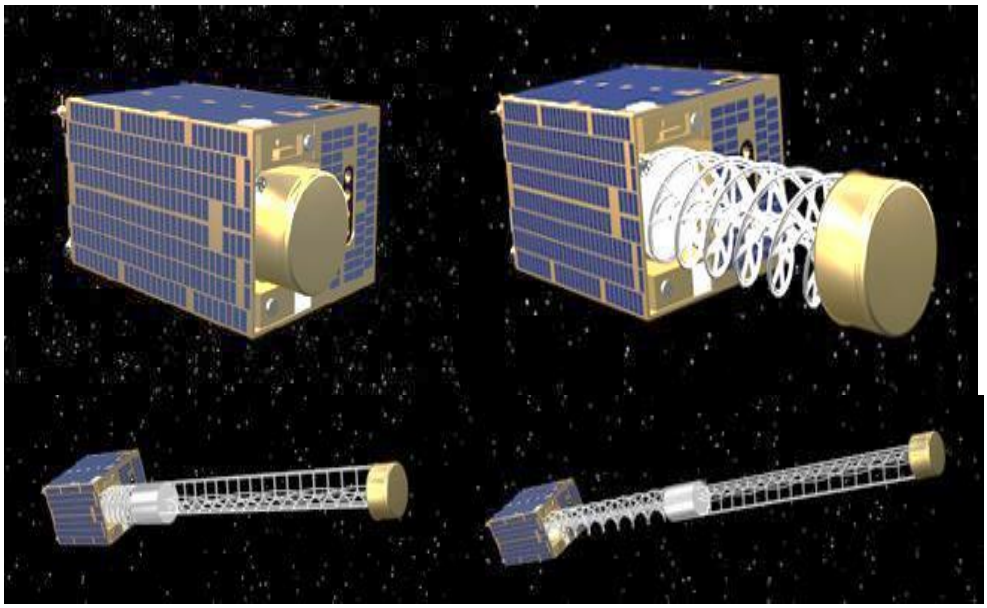

Figure 1.1: Deployment of Ørsted satellite (courtesy: DNSC)

Even though the deformable booms with ultrathin composites conquer the aforementioned limitations, folding of such structures are limited to their elastic regime. Once the folding is extended beyond the elastic region, these composites are either subjected to fibre failure or to plastic deformation of matrix [5]. Composites made with soft elastomeric matrix like silicone is capable of complete recovery of deformation after subjecting to extreme curvatures by eliminating these issues through fibre micro-buckling [6]. Dual-matrix fibre composites, where traditional epoxy matrix is replaced with a soft-elastomer (silicone) in highly deformable regions, were invented to drastically improve the performance of elastically deformable deployable structures. Thus the structures made of dual-matrix composites can entertain high curvatures up to 180^0 fold without any fibre or matrix failure [7]. However it has been reported that dual-matrix composites demonstrate a significant reduction in bending stiffness under extreme curvatures and presently being under investigation.

1.2. Physical Testing of Deployable Structures

Deployment behaviour of a deployable structure can be significantly affected when tested on Earth due to gravitational acceleration which is not present in space. Often gravity offload systems are used to reduce the gravitational effects when testing motorized structures. However, when it comes to ultrathin fibre composite booms which are designed to self-deploy using the stored energy is far more challenging. Effects like gravity, friction and air drag can simply prevent a structure from deploying. Drop towers and reduced gravity flights are two more advanced testing facilities that are being used to simulate reduced gravity environment for small structures with very short deployment time (seconds). Drop tower test is used when the devices are rough enough to survive weightlessness free fall or inexpensive to replace every time after a fall [5], [6]. For large space structures, which have longer deployment period, zero-gravity flights are being used. As shown in Figure 1.2 an airplane flying in a parabolic path experiencing zero-gravity condition for a duration about 25 seconds. However it should be noted that still the air drag is present inside the airplane and that can change the real deployment behaviour of the structure.

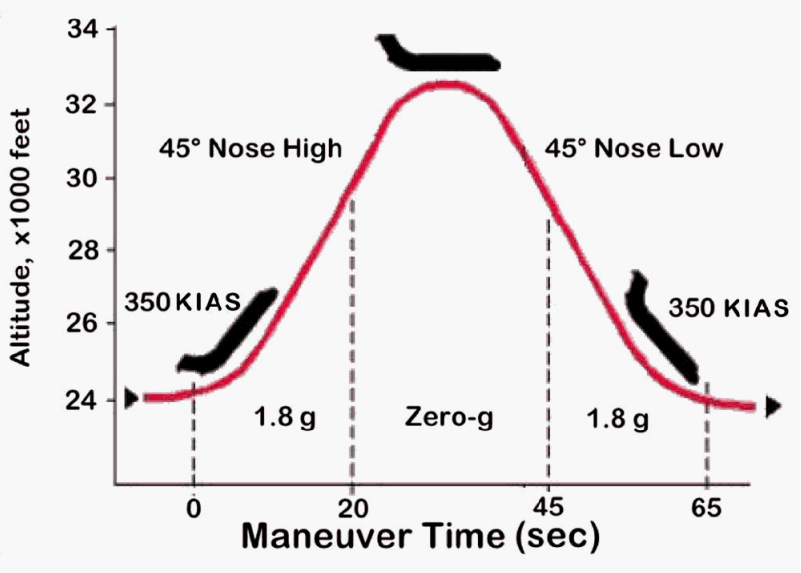

Figure 1.2: Reduced gravity flight (courtesy: NASA)

1.3. Analytical models and Virtual Simulations

Apart from the above mentioned drawbacks, physical testing is very expensive and time consuming. Considering these factors, two alternative methods are available for design optimization using several design cycles before the final physical testing as described below.

The first method is to make an analytical model of the structure. Calladine [7] has shown the ability to capture bending energy of a coiled boom using a purely analytical model. However, analytical approaches impose issues in capturing contacts, resulting in snapping and large deformations in the geometry under dynamic conditions which are critical for deployable booms.

The second approach is to create numerical models to simulate deployment behaviour using finite element analysis. High performance computers and robust solver algorithms in commercially available finite element software packages have made it possible to create virtual models capturing dynamic snapping and advanced contact behaviour.

1.4. Objective and Scope

As described above it is essential to have virtual simulation techniques which can predict folding/deployment behaviour of dual-matrix composites for the optimization of future space structures. This research focuses on predicting deployment behaviour of dual-matrix booms made of thin fibre composite using virtual simulations. Effect of nonlinear bending stiffness variation with degree of deformation of the fibre-elastomer is studied via modifying the shell section definition in Abaqus/explicit finite element package. The study is limited to deployable booms made of three-ply plain-woven fibre composites.

1.5. Layout of Thesis

This thesis comprises of 6 chapters, including the first introductory chapter.

Chapter 2 gives a brief review of the composite and past studies on self-deployable booms. The first part of the chapter explains analytical methods of predicting mechanical properties and micro buckling in large strain composites. Next, characterization of tape-springs and booms using moment-rotation response is discussed. The last part of the chapter reviews the case study experiment used for the verification.

Chapter 3 describes the finite element model and simulation technique developed to predict quasi-static deployment behaviour. An introduction for the commercially available Abaqus/Explicit finite element package with available features, key parameters to investigate and necessary checks is presented. A series of independent folding and deployment simulations with predefine constant bending stiffness properties was analysed to predict the effect on moment-rotation characteristics of a boom.

Chapter 4 presents the results of the simulation for dual-matrix composite boom made of thin fibre composite. Comparison of moment-rotation response for quasi-static simulation with different bending stiffness is highlighted.

Chapter 5 explains the simulation techniques to account for variable bending stiffness using import analysis. Three different analyses were performed to investigate the possibility of changing bending stiffness at predefined stages of the analysis.

Chapter 6 presents the basics of user subroutine which is used to change the bending properties during an analysis. Sensitivity analysis was performed to predict membrane stresses for a solid model using user subroutines. Further a method to simulate shell behaviour of a plate using subroutine is investigated.

Chapter 7 concludes the thesis and suggests recommendations for future work.

CHAPTER II

2. Literature Review

This chapter presents general overview on composite material and characterization of deployment behaviour. The chapter starts with an introduction to composite material and focuses on fibre composite material with analytical prediction of stiffness matrix. The second section focuses on characterization of booms and tape springs using moment-rotation curve to understand deployment behaviour. In the final section the dual-matrix composite boom with quasi-static experiment and simulation to characterize behaviour of boom are explained.

2.1. Composite Material

The word composite in the composite material expresses the idea of combining two or more materials in order to produce a new type of material. This combination is performed in macroscopic scale wherein the components can be distinguished by naked eye. If composites are well designed, they possess the best qualities of parent materials and often some qualities that neither of them shows. Constituent materials can be significantly different resulting composites to be heterogeneous at microscopic scale. But in macroscopic scale material is statically homogeneous. Some of the characteristics that can be improved in composite materials are strength, stiffness, corrosion resistance, wear resistance, fatigue life, thermal insulation and acoustic insulation.

Not all these properties can be improved at the same time. Most cases, the objective is developing the perfect material for one unique task. That purpose can be achieved with composites.

Fabrication of composites runs to the prehistoric era and it is considered as one of the oldest engineering methods. At first composites like straw reinforced mud and plywood were used by earliest civilization once they realized the improvement of physical properties of these. Present day composites can be found everywhere around us. Range of usage run through the day to day utensils to the aerospace and military applications.

There are four commonly accepted types of composites materials. This categorization is characterized by the method of combining materials [8].

1. Fibrous composites – consist of fibres in a matrix (Ex. Fibre glass)
2. Laminated composites – consists of layers of various materials (Ex. Bi-metals)
3. Particulate composite – composed of particles in a matrix (Ex. Concrete)
4. Combination of some or all of the above types (Ex. Woven fibre composites)

2.1.1. Fibre Reinforced Composites

From these categories, fibre-reinforced composites (FRC) are the most demanding type in aerospace and military industries due to its lightweight, high stiffness to mass ratio, high strength to mass ratio and the ability to tailor to achieve required material properties. Due to the increasing popularity of FRC, it is needed to understand the micro mechanical behaviour of such composites clearly.

A FRC is manufactured by stacking a certain number of anisotropic layers which are called as lamina or ply. FRC lamina can be made of unidirectional or woven fibres with different fibre orientations depending on design and draping requirement.

Unidirectional ply has continuous fibres that majorly run in one direction only. But small amount of fibre or other material may run in other direction, mainly to hold primary fibres in position.

Woven composites are produced by weaving tows or yarns of a particular fibre and impregnating it in a resin matrix. This resin system holds the woven fabric together and transfers mechanical loads through the fibres. As the name implies woven composites differ with each other based on their weave pattern such as plain weave, satin weave, twill weave, etc. (see Figure 2.2) Laminates can be made with several layers of unidirectional in different orientations or woven plies as shown in Figure 2.1.

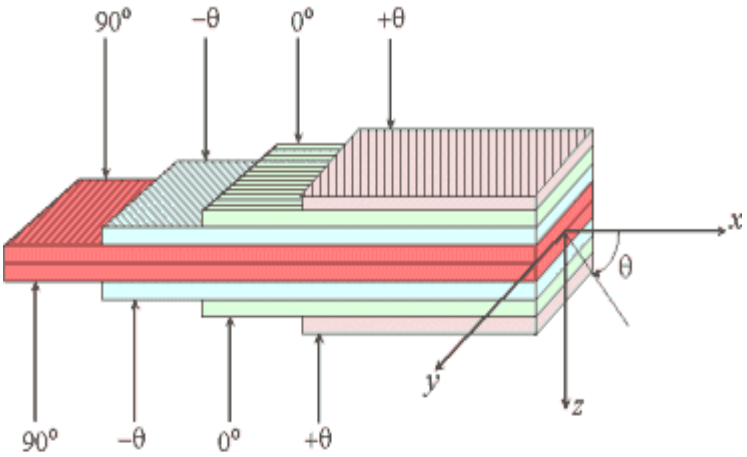

Figure 2.1: Laminate made of unidirectional lamina placed at different orientations

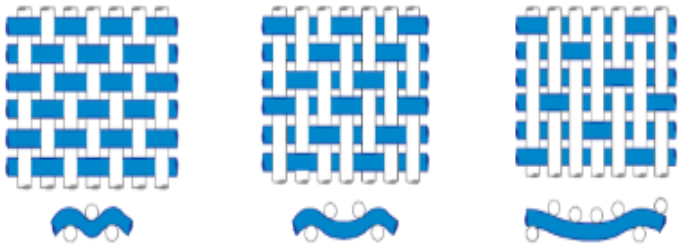

Figure 2.2: Woven plies

2.1.2. Analytical Prediction of ABD Matrix

Characterization of mechanical behaviour in laminates are done by studying micro-mechanical models of individual plies. Since the fibre composites are formed with several anisotropic layers to achieve the desired material properties, Classical lamination theory (CLT) is commonly utilized to obtain the effective properties of the laminate. This constitutive relationship is presented in terms of 6x6 matrix called as ABD matrix [9]. The ABD stiffness matrix defines the relationship between in-plane forces (N_x, N_y, N_{xy}) and out-of-plane moment resultants (M_x, M_y, M_{xy}) (see Figure 2.3) with mid-plane strains (ε_x, ε_y, γ_{xy}) and out-of-plane curvatures (κ_x, κ_y, κ_{xy}) as given in the equation 1.

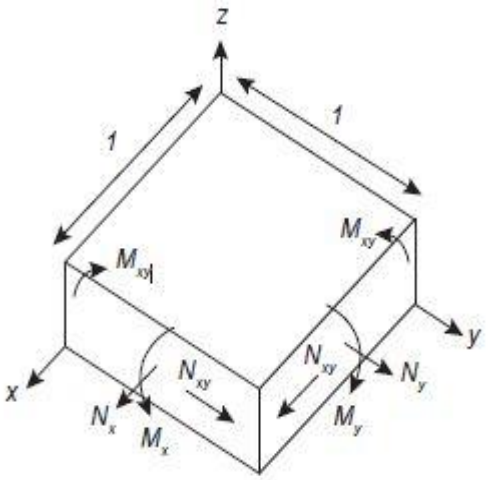

Figure 2.3: Notation for resultant directions of forces and moments

$$\begin{Bmatrix} N_x \\ N_y \\ N_{xy} \\ \hline M_x \\ M_y \\ M_{xy} \end{Bmatrix} = \begin{pmatrix} A_{11}\ A_{12}\ A_{16} & | & B_{11}\ B_{12}\ B_{16} \\ A_{21}\ A_{22}\ A_{26} & | & B_{21}\ B_{22}\ B_{26} \\ A_{61}\ A_{62}\ A_{66} & | & B_{61}\ B_{62}\ B_{66} \\ \hline B_{11}\ B_{12}\ B_{61} & | & D_{11}\ D_{12}\ D_{16} \\ B_{12}\ B_{22}\ B_{62} & | & D_{21}\ D_{22}\ D_{26} \\ B_{16}\ B_{26}\ B_{66} & | & D_{61}\ D_{62}\ D_{66} \end{pmatrix} \begin{Bmatrix} \varepsilon_x \\ \varepsilon_y \\ \gamma_{xy} \\ \hline K_x \\ K_y \\ K_{xy} \end{Bmatrix} \quad (1)$$

The sub 3x3 matrices denoted by A, B and D for a laminate of n plies can be determined in terms of the ply stiffness, $\bar{Q}$, which includes details about orientation of the fibre in the ply [10], [11].

$$\text{A} = \sum_{i=1}^{n} \bar{Q}_i (z_{i+1} - z_i) \quad (2)$$

$$\text{B} = \frac{1}{2} \sum_{i=1}^{n} \bar{Q}_i ({z^2}_{i+1} - {z^2}_i) \quad (3)$$

$$\text{D} = \frac{1}{3} \sum_{i=1}^{n} \bar{Q}_i ({z^3}_{i+1} - {z^3}_i) \quad (4)$$

Even though the in-plane properties of woven composites can be accurately predicted [12], the bending property estimations shows errors up to 200% in the bending strains and up to 400% in bending stiffness. Researchers have shown that the CLT, which assume ply is orthotropic in fibre direction and homogeneous through thickness can significantly overpredict the bending stiffness when it comes to ultra-thin weave laminates, since ply is not homogeneous through thickness.

Due to the aforementioned reasons, determination of micro mechanical behaviour is troublesome using the available theories and methods. Using of Classical Lamination Theory (CLT), which is used to analyse the mechanical behaviour of laminates, shows very high error margins in bending stiffness for thin fibre composites which are made up of single to two plies. Therefore recently researchers tend to go for micromechanical modelling using representative unit cell in order to obtain the ABD stiffness matrix coefficients by using virtual work principles. A model with a modification to CLT is proposed by the MOSAIC model [12] in order to account for thin plain-weave laminates. Figure 2.4 shows the proposed model, where each lamina is modelled as a repeating unit cell with two layers of tiles of weft yarns and warp alternatively [13]–[17].

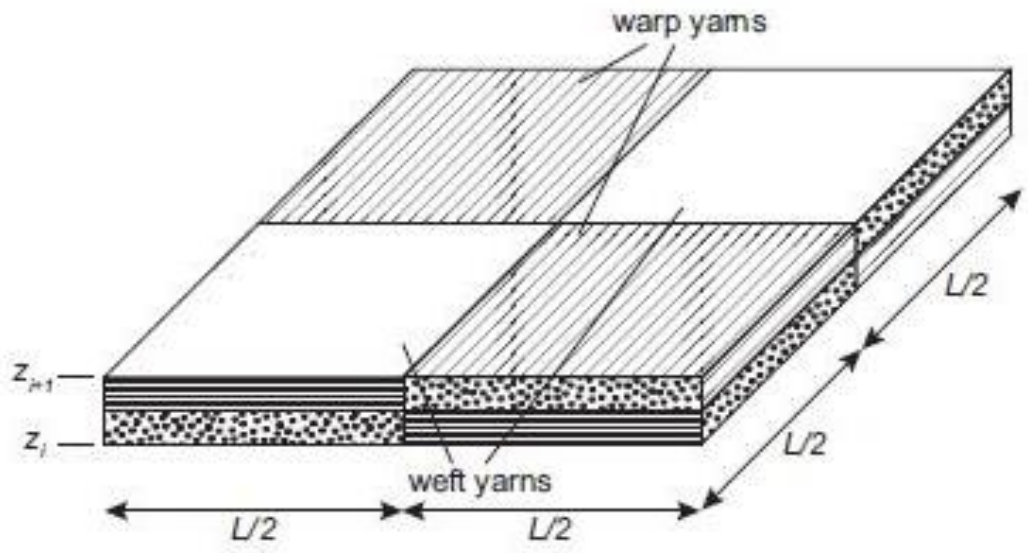

Figure 2.4: Mosaic unit cell model with plain – weave approximation

For the unit cell, ABD stiffness matrices can be calculated using following equations,

$$A= \sum_{i=1}^{n} \frac{1}{2}(\bar{Q}_i^{0^0} + \bar{Q}_i^{90^0})(z_{i+1} - z_i) \quad (5)$$

$$B= 0 \quad (6)$$

$$D= \frac{1}{3}\sum_{i=1}^{n} \frac{1}{2}(\bar{Q}_i^{0^0} + \bar{Q}_i^{90^0})(z^3{}_{i+1} - z^3{}_i) \quad (7)$$

Where B sub matrix is equal to zero due to symmetry. In equations 5-7, it is visible that for lamina stiffness, $\bar{Q}$ is given as an average of warp and weft tile stiffnesses.

It has been found that, usually this theory is able to approximate in-plane stiffness in laminates. But in thicker layups, this method can give errors up to 100% when estimating bending stiffness due to introducing discontinuities in fibres by neglecting undulation in the yarns [12].

2.1.3. Large-Strain Fibre Composites

Especially in aerospace industry, use of rigid assemblies with mechanical hinges that are associated with motors and springs for actuation lead to higher weight and increased complexity [18], [19]. Elastically deformable thin fibre composites that are capable of deploying with stored energy has been introduced as a feasible alternative for these weight sensitive applications [3], [20]. Even though the deformable structures with ultrathin composites conquer the aforementioned limitations, folding of such structures are limited to their elastic regime. Once the folding is extended beyond the elastic region, these composites are either subjected to fibre failure or to plastic deformation of matrix [21], [22]. For fibre composites made of traditional epoxy, the failure radius is in between 5 mm – 10mm.

However, after conducting many researches, large-strain composites with continuous reinforcement fibres embedded in soft matrix have been proposed as an alternative composite material softer than epoxies. Composites made with soft elastomeric matrix like silicone is capable of complete recovery of deformation without permanent damage after subjecting to extreme curvatures by eliminating above mentioned issues through fibre micro-buckling [23]–[25].

Figure 2.5 [26] demonstrate the micro-buckling of fibres on compression side in a highly deformed elastic memory composite. Furthermore, Murphey et al. [25] describes this stress relieving mechanism in micro-buckling (See Figure 2.6). When folding starts, for small bending curvatures, extensional stiffness will remain uniform through thickness prior to buckling and hence neutral axis lies in the laminate mid-plane. As the critical buckling load is reached by fibres on the compression side of the

laminate, their stiffness drastically reduced in the post-buckling range which produces a bilinear constitutive model that shifts the neutral axis towards the tensile side from the middle plane of the laminate. This results in a reduction of the maximum tensile and maximum compressive strain in the fibres allowing them to withstand high curvatures by remaining elastic than if the fibres had remained unbuckled.

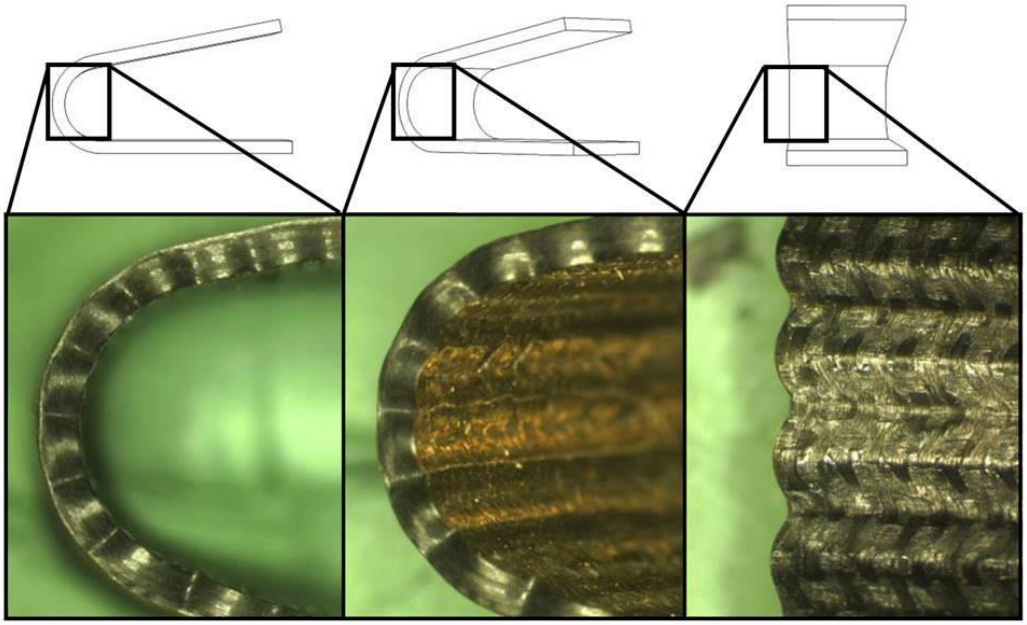

Figure 2.5: Micro-buckling of fibres on compression side in a highly deformed elastic memory composite [26]

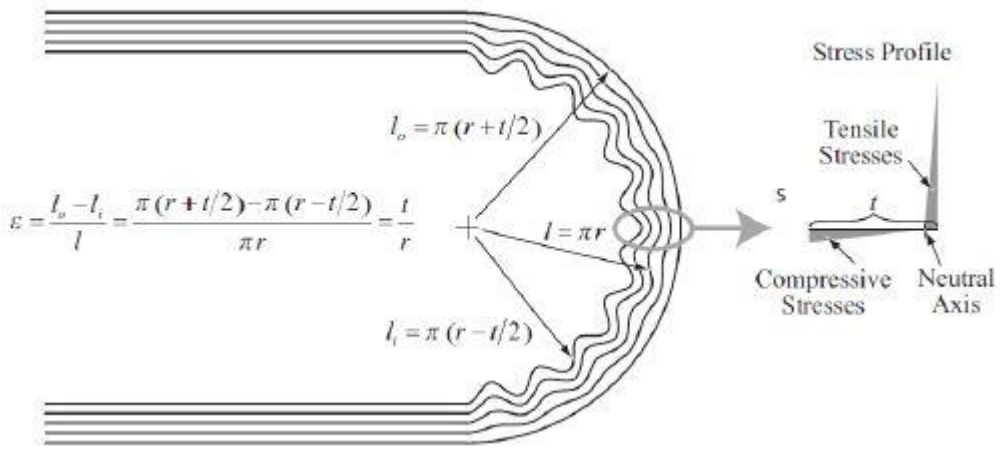

Figure 2.6: Fibre micro-buckling and stress profile in a highly bend UD laminate [25]

2.1.4. Dual-Matrix Composite

Self-deployable booms made of thin fibre composites with rigid matrix like traditional epoxy, cannot undergo high curvatures with typical failure radius between 5 mm to 10 mm. This has limited the compacting ability of structures to fit into launching vehicles with very small degree of compaction as in Figure 2.7.

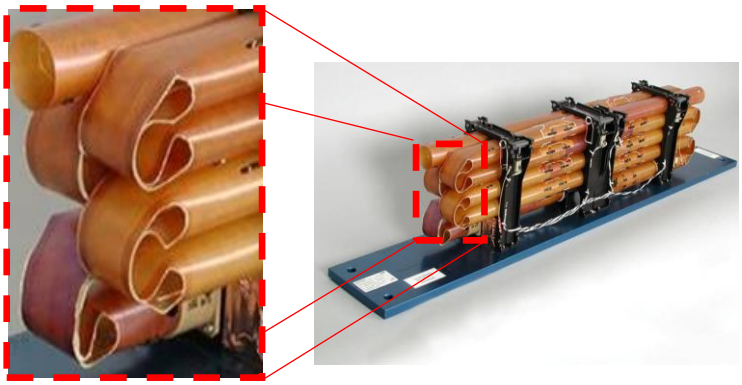

Figure 2.7: MARSIS antenna boom structure (courtesy: Astro Aerospace)

Researches have been carried out to find a solution for that and booms with open cross-sections have been studied [27]–[33]. But these booms are weak in torsion and hugely reduce structural performance of structures.

Figure 2.8: Carbon fibre lightweight boom with longitudinal slots [29]

Another proposed method is connecting two tape-springs with an adhesive to make a closed-cross section boom as in figure 2.9 [34]–[36]. Here, it is needed to control boom deployment very carefully to stop chaotic deployment due to stored excessive strain energy and the use of adhesive to glue tape-springs make manufacturing process complicated.

Figure 2.9: CFRP composite boom (courtesy: DLR)

With new advancement of technology, it is possible to fold soft elastomers into very high curvatures without damaging material. However, use of soft elastomeric matrix composites such as Carbon Fibre Reinforced Silicone (CFRS) for deployable structures in space applications are limited due to stability issues in deployed structural performance and inability to store enough strain energy to self-deployment when released. New composite material for thin-walled deployable structures with two matrices has been introduced by Karl [26] increasing the structural efficiency while allowing deformation for high curvatures.

Dual-matrix fibre composites, where traditional epoxy matrix is replaced with a soft-elastomer (silicone) in highly deformable regions, were invented to drastically improve the performance of elastically deformable deployable structures. Thus, the structures made of dual-matrix composites can entertain high curvatures up to 180^0 folds without any fibre or matrix failure. Fibre damage during folding is prevented as the fibres on the compression side of the fold undergo micro buckling [26]. However the mechanical properties of the dual-matrix composites have not been studied in detail and it is extremely important to understand the behaviour under high curvatures.

2.2. Characterizing Tape Spring Hinges

Research has shown that behaviour of a tape spring can be characterised by a moment-rotation relationship *M (θ)*, (see figure 2.10) to understand the folding and deployment response in a particular structure [37], [38]. Typical tape-spring has a geometry shown in figure 2.11. The initial unfolded configuration is denoted by O at the origin. A single tape-spring can be bent in opposite-sense bending or equal-sense bending, as illustrated in figure 2.12. In opposite-sense bending figure 2.12 (a), positive bending moment induces tension along the edges of the tape spring.

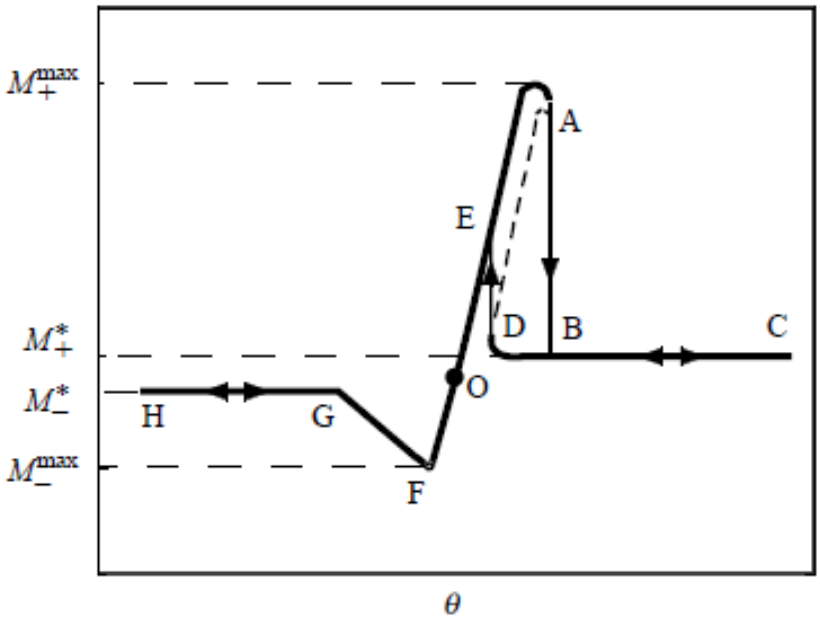

Figure 2.10: Moment-rotation relationship of a tape-spring

At the beginning, for small rotation angles, moment-rotation relationship of tape-spring shows a linear behaviour from O to A until the tape spring suddenly snaps at A and buckles into two approximately straight sections connected by a localized fold. From B to C arc length of localised fold increases but its radius shows no change, while the bending moment is constant. During unfolding process, from C to D the tape-spring follows the constant moment path until suddenly snaps at E. For negative moments in equal-sense bending (see Figure 2.12 (b)), which induce compressive stresses along the edges of the tape-spring, moment-rotation response is linear but end sooner compared to opposite-sense bending because of sudden bifurcation occurring at F, corresponding to a flexural-torsional deformation of the whole tape spring.

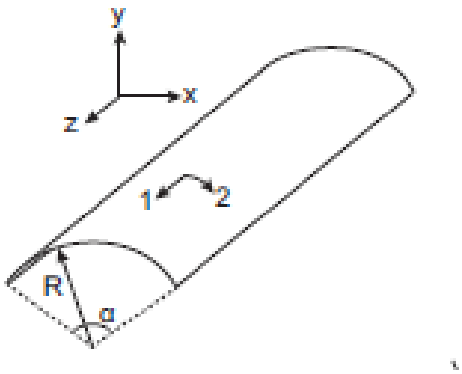

Figure 2.11: Single tape spring geometry

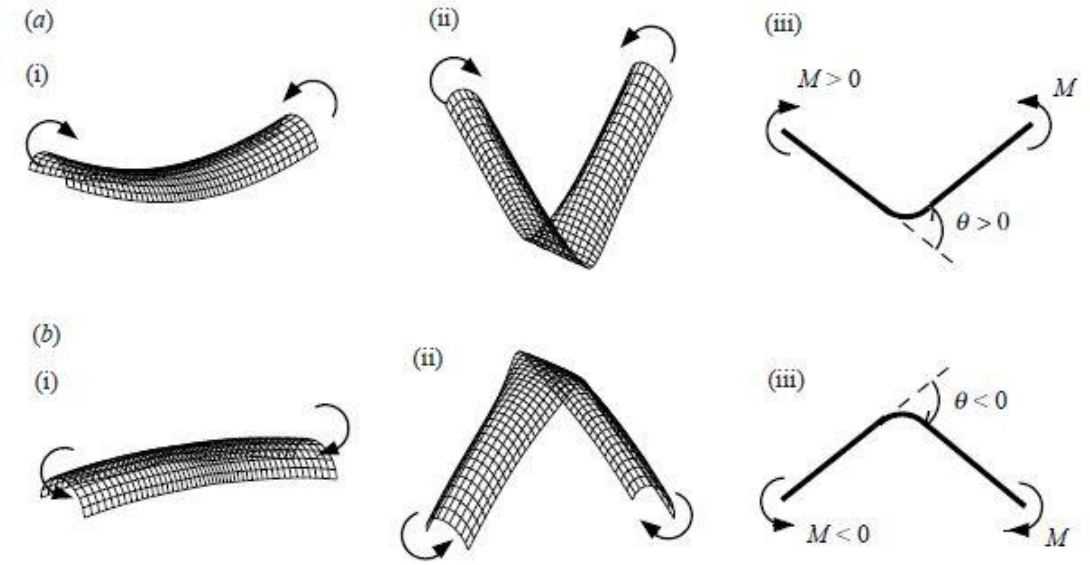

Figure 2.12: Bending of tape-spring s (a) opposite-sense (b) equal-sense

For a self-deployable closed cross section boom, similar characterization can be done using moment-rotation relationship, where two tape-springs are connected in opposite orientation. In this case one tape-spring undergoes equal-sense bending while the other one undergoes opposite-sense bending and behaviour can be predicted using superposition of two separate cases described above [39].

However during folding, the folding angle of the outer tape-spring is smaller than the inner tape-spring due to assembly between tape-springs. This can lead to two different moment peaks with the buckling of inner tape-spring at first, upon folding.

For the bending in opposite direction, moment-rotation graph shows identical response as a result of symmetry with two distinct moment peaks (see Figure 2.13).

When rotation angle $\theta < \theta_1$, two tape-springs show a linear behaviour. After moment reaching to M_1^+ boom suddenly snaps and drop the moment to M^+ while starting to make a localized elastic bend. Then, as the rotation is increased, the moment shows a small rise with the buckling of outer tape-spring to reach smaller peak M_2^+ and again drop to M^* with further rotation. For further increase in rotation, localized fold remains unchanged and the steady state moment remains constant which is approximately equal to M^*.

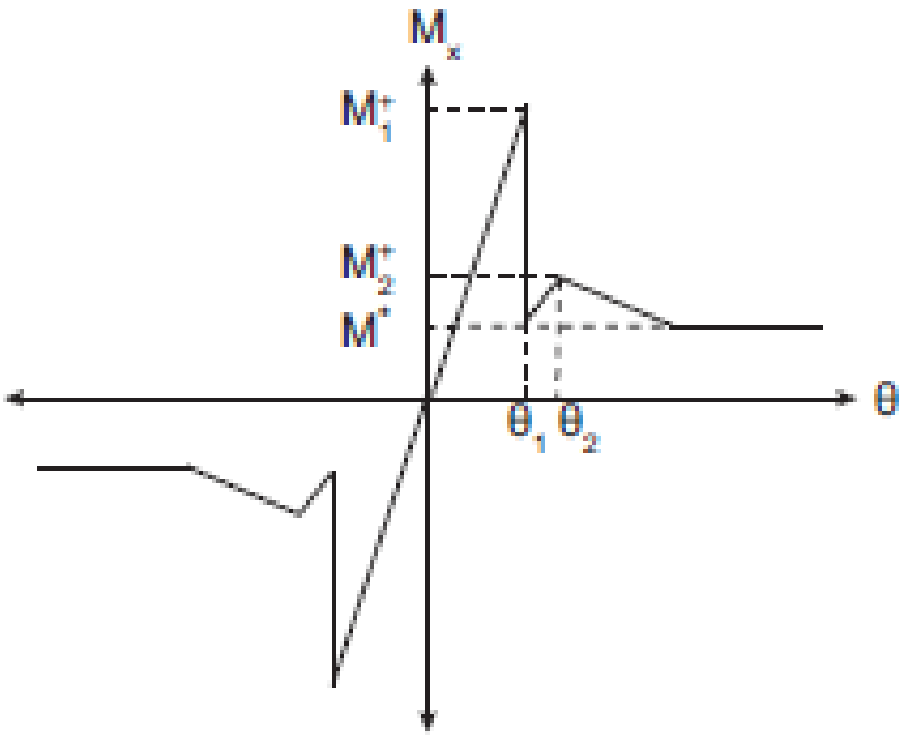

Figure 2.13: Predicted Moment-rotation relationship two tape-springs

2.3. Dual-Matrix Composite Boom

Quasi-static deployment behaviour of dual-matrix composites was studied by Sakovsky et al. [40] using a closed cross-section dual-matrix composite boom made of 3-ply plain weave glass fibres, which is 250 mm long and 25.4 mm in diameter. The symmetric $[45/0/45]_{p\text{-}w}$ layup had a thickness of 0.3 mm and was fabricated using Astroquartz (AQ) II plain-weave (p-w) fabric. Loctite 5055 UV-cure silicone as the elastomer matrix in the hinge region and PMT-F4B epoxy elsewhere were used as shown in figure 2.14.

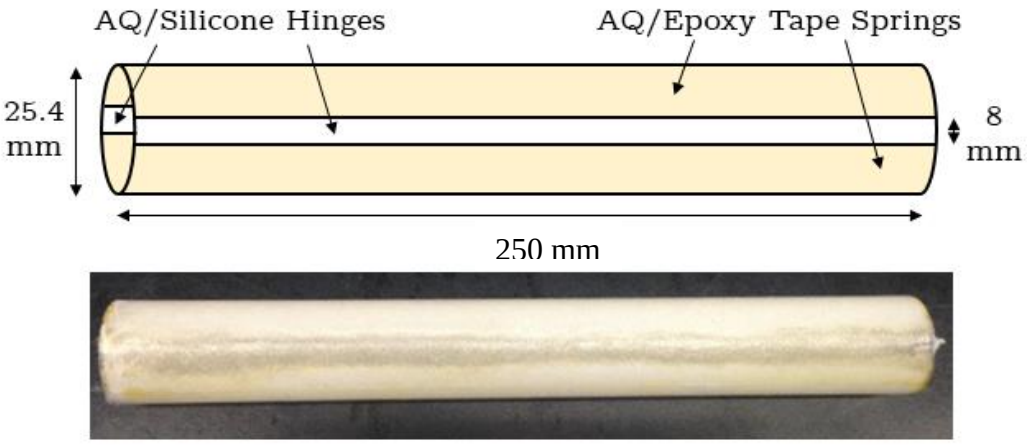

Figure 2.14: Dual matrix composite boom

2.3.1. Quasi-Static Deployment Experiment

Figure 2.15 shows the experimental setup that has been used by Sakovsky et al. [40] to measure moment-rotation response to characterize dual-matrix boom. Two strips at both ends of the boom were rigidly connected to two holders, whose rotation can be controlled using gears, allowing ovalization of cross-section during folding. Right arm was restrained in translation while the left arm was free to slide in a linear path by a guide bearing to simulate pure-bending behaviour. Strain gauges attached to rigid holders were used to measure the moment response.

Boom was first pinched by hand at the centre to avoid any damage to the fibre and folded to $\theta = 100^0$ by rotating the handles attached to two gears on either end. Once the required folding configuration has been achieved, both gears were rotated

back in small steps while recording the moment on either end. Figure 2.16 shows the measured moment–rotation response of the boom. Note that the deployment angle is defined as the angle between the two axes of straight portions of the boom. The measured steady state moment was 34 Nmm, which is the average moment for $40^0 < \theta < 100^0$. The peak moment was recorded as 634 Nmm at $\theta = 7^0$.

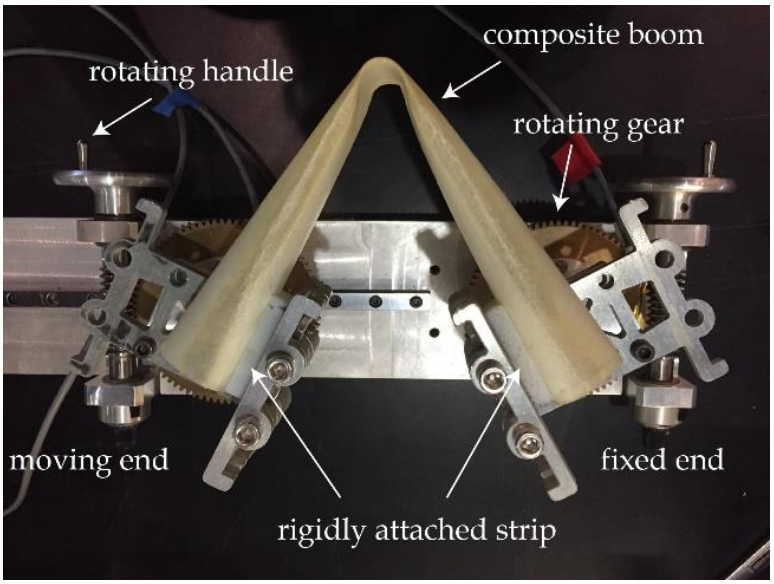

Figure 2.15: Experimental setup used by Sokovsky to measure moment response of dual-matrix composite boom during deployment [40]

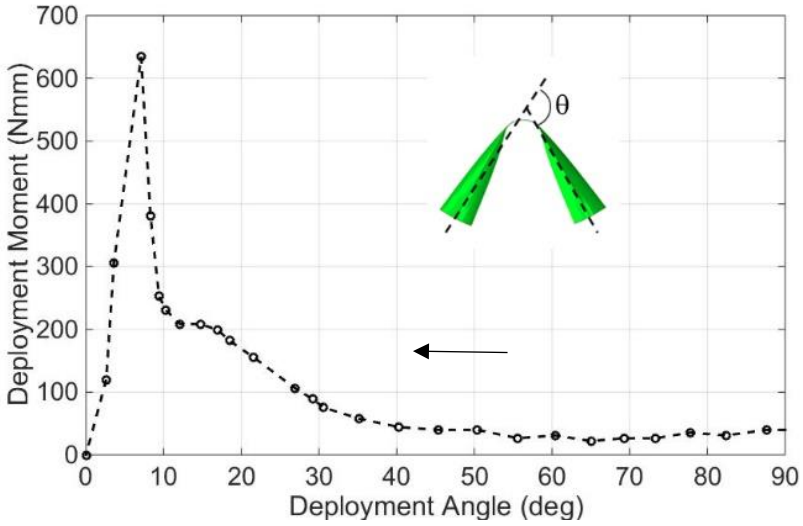

Figure 2.16: Experimental Moment-rotation response of dual-matrix composite boom [40]

2.3.2. Quasi Static Deployment Simulation

An attempt was made by Sakovsky et al. [40] to simulate deployment behaviour of dual-matrix composite boom using finite element analysis. Three different idealizations were tried where, the silicon hinge modelled with M3D3 membrane elements without a bending stiffness, as a perfect hinge and using S4 shell elements specifying ABD stiffness matrix corresponding to silicone. Generally, all three approaches showed huge variation when comparing simulated moment-rotation response with experimental observations. Only the third approach agreed with experimental results for some extent, capturing overall deformed configuration with an acceptable accuracy.

Following Sakovsky et al. [40], Ubamanyu et al. [41] have made an attempt to simulate dual-matrix composite boom. When the bending stiffness of silicon region is reduced to 10% of the initial value, simulation is capable of capturing localized hinge deform configuration and steady-state moment for, $40^0 < \theta < 100^0$ with a good agreement (see Figure 2.17). But results show a weaker response in the moment, for deployment angle, $0^0 < \theta < 40^0$. Also the peak moment when snapping is not captured accurately.

It was decided to follow similar simulation approach modifying key parameters by understanding limitations to increase accuracy of moment-rotation response. Since the behaviour of dual-matrix composite boom depends on the change of bending stiffness in elastomer due to micro-buckling, detail investigation was done to understand the effect of variable bending stiffness for different curvature in simulation results. Furthermore, development of a simulation technique to incorporate variable bending stiffness rather than using a constant stiffness value throughout the simulation has been proposed in the subsequent chapters.

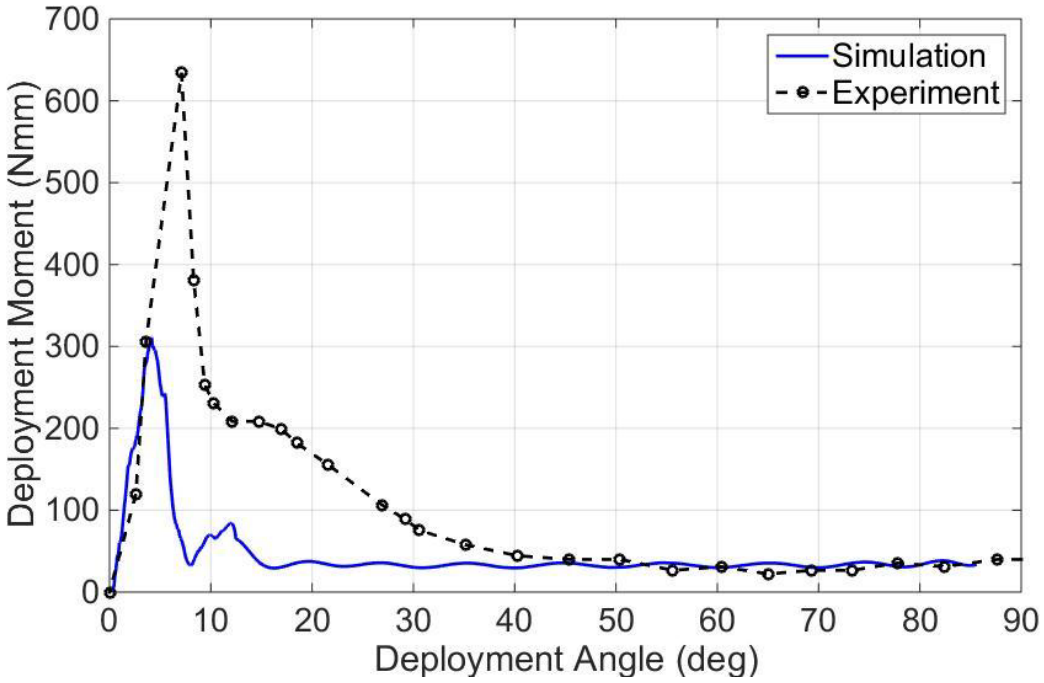

Figure 2.17: Comparison of simulated moment-rotation curve [41]

CHAPTER III

3. Dual Matrix Hinge

In this chapter, finite element technique adopted to simulate deployment behaviour of closed cross-section dual-matrix composite boom is discussed. The experimental study carried out by Sakovsky et al. [40] which was explained in detail under Chapter 2 was used as a case study for the simulation. The quasi-static deployment behaviour was predicted using Abaqus/Explicit, commercially available finite element software which uses robust algorithm including many other features.

At the beginning of the chapter, detailed description of finite element model of dual-matrix composite boom is provided. Then, the chapter explains different simulation parameters and checks that are necessary to achieve numerically accurate simulation technique. Finally, sequence of the simulation process for folding and deployment with selected key parameters is explained.

3.1. Finite element model

Figure 3.1 shows the finite element model of the dual-matrix composite boom used to simulate quasi-static response of folding and deployment behaviour which was created using commercial finite element software package Abaqus/Explicit.

Boom was partitioned to separate the silicon region from epoxy. 8 mm wide silicon region was meshed with a finer mesh towards the middle of the boom, where it is subjected to high curvatures. The epoxy region was meshed finer towards the centre and much coarser towards the ends to be compatible with the mesh in the silicone region while reducing the computational cost. The finite element model consisted of 10577 nodes and 10536 four-node doubly curved shell elements with full integration (S4) with minimum element size of 0.75 mm as shown in Figure 3.1. S4 elements were used to model the boom instead of quadrilateral elements with reduced integration (S4R) to avoid build-up of artificial energy due to hourglassing. However, as described in the next section fully integrated first order elements can create the numerical problem called shear locking. To prevent that, model was created using S4 second order elements for better accuracy.

The material properties of the ABD stiffness matrices for Epoxy and Silicon shell elements were defined with **Shell General Section* keyword in Abaqus with the material orientations x and y (longitudinal and circumferential respectively) as defined in Figure 3.1. Equations 8 and 9 give the constitutive relationships of AQ/Epoxy and AQ/Silicon under small deformations, respectively.

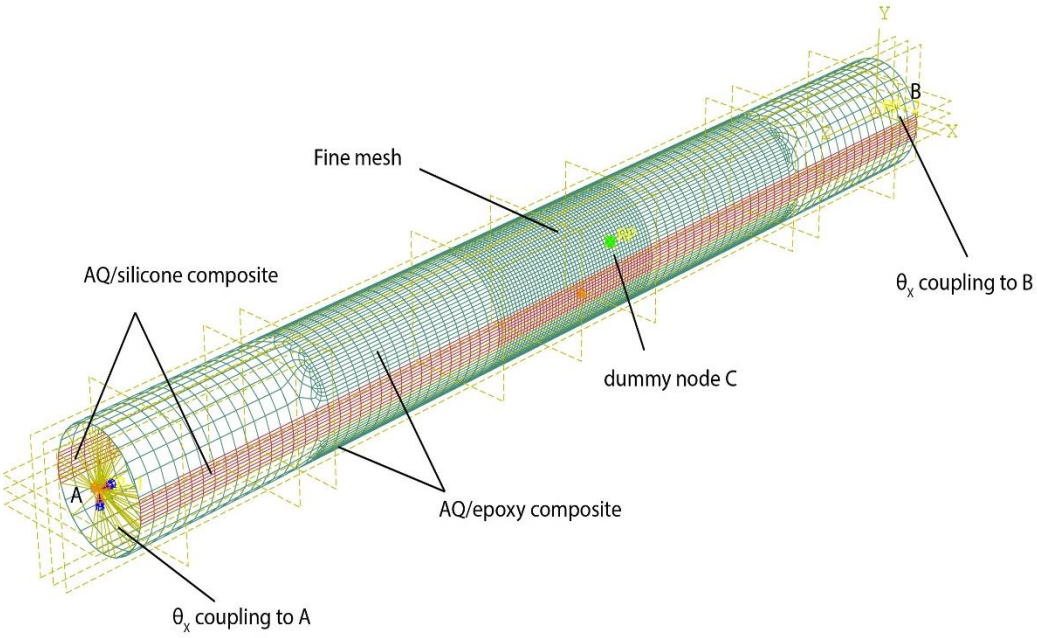

Figure 3.1: Finite element model

$$ABD_E = \left(\begin{array}{ccc|ccc} 2569 & 972 & 0 & 0 & 0 & 0 \\ 972 & 2569 & 0 & 0 & 0 & 0 \\ 0 & 0 & 1128 & 0 & 0 & 0 \\ -- & -- & -- & -- & -- & -- \\ 0 & 0 & 0 & 4.3 & 2.4 & 0 \\ 0 & 0 & 0 & 2.4 & 4.3 & 0 \\ 0 & 0 & 0 & 0 & 0 & 2.7 \end{array}\right) \quad (8)$$

$$ABD_s = \left(\begin{array}{ccc|ccc} 1809 & 945 & 0 & 0 & 0 & 0 \\ 945 & 1809 & 0 & 0 & 0 & 0 \\ 0 & 0 & 945 & 0 & 0 & 0 \\ -- & -- & -- & -- & -- & -- \\ 0 & 0 & 0 & 6.2 & 5.8 & 0 \\ 0 & 0 & 0 & 5.8 & 6.2 & 0 \\ 0 & 0 & 0 & 0 & 0 & 5.8 \end{array}\right) \quad (9)$$

Units are in N and mm for both matrices.

In the experimental study carried out by Sakovsky et al.[40], it was observed that there is an ovalization of cross-section during folding at the end of the boom closer to two holders. Therefore, it was required to impose similar boundary conditions in finite element model to achieve accurate simulation results. If rigid constraints were used, it would have prevented any deformation of the cross-section and may lead to significantly varied results. To avoid this coupling constraints were defined using **Coupling* Abaqus key word at both ends of the boom, allowing cross-section to freely deform into oval shape during folding. 10 mm strips at either end of the boom were connected to two reference nodes A and B using *Kinematic *4, 4* Coupling constraints to couple the rotations about X-axis which is represented by fourth degree of freedom (θ_X).

These reference points were then connected to a dummy node C to simulate pure bending behaviour through an **Equation* constraint command as shown in equation 10 to induce equal end moment conditions. Except for rotation about X-axis, all degrees of freedom at node A are prevented. Node B is allowed to translate along Z-axis following the experimental setup along with rotation about X-axis while restraining other degrees of freedom.

$$\theta_X^A - \theta_X^B = \theta_X^C \quad (10)$$

Where θ_X represent rotation about the global X-axis

The **General contact* feature in Abaqus/Explicit, which automatically detects the potential contact surfaces around the whole hinge surface was used to define the frictionless contact behaviour between interacting bodies to the entire model using *Contact Inclusions, All Exterior*.

3.2. Abaqus/Explicit Simulation Techniques

The initial purpose of developing explicit solver was to model high speed dynamic events with high inertia forces. Explicit solver uses forward Euler integration method combining diagonal or lumped mass matrices M, to solve equation of motion by calculating acceleration easily at any given time t, using following equation.

$$\ddot{U}_{(t)} = |M^{-1}(P - I)|_{(t)} \tag{11}$$

Where P and I are external load vector and internal load vector respectively.

Apart from the main purpose of Abaqus/Explicit to solve for true dynamic equilibrium, nowadays it has been used to solve highly nonlinear static problems. Explicit has proven the suitability for Quasi-Static simulations by using fewer computational cost compared to implicit solver, when very large deformations and complicated contacts are present in models.

Folding and deployment simulations of dual-matrix composite-booms involve very large non-linear geometric changes with dynamic snapping and extensive contact between surfaces, which is better simulated by explicit solver than implicit. However above mentioned phenomena could result in numerical instabilities and convergence issues due to singularity in stiffness matrix. To avoid the limitations, different approach of explicit procedure which advances the kinematic state of each degree of freedom in calculation of stiffness matrix is adapted by direct integration of its equation of motion.

Special focus was given to control three independent techniques for stability of explicit solution, time increment, loading rate and numerical damping. Shear locking phenomena was also addressed for the model to be free from any numerical instability. Optimization of model parameters was done after studying effects and limitations of those key factors.

3.2.1. Stable Time Increment

In explicit procedure every problem is solved as a wave propagation problem where out-of-balance forces are propagated as stress waves between contiguous elements.

It is convenient to have large integration time increment to reduce the number of increments needed to complete the simulation. However, in order to capture stress waves between neighbour elements the Courant stability condition should be satisfied [42]. It indicates that, the time increment should not exceed the time for a wave to travel across adjacent nodes in explicit analysis. Central difference operator is conditionally stable, but the magnitude of numerical damping will influence the stable time increment and it can be seen that increasing damping will reduce the stable time increment. When the damping is used to control high oscillations in the system, the stability limit can be specified in terms of the highest eigenvalue in the system as given below.

$$\Delta t \leq \frac{2}{\omega_{max}}\left(\sqrt{1-\xi^2}-\xi\right) \tag{12}$$

This condition can be considered as an approximate relationship for minimum stable time increment as,

$$\Delta t = \propto \left(\sqrt{1-\xi^2}-\xi\right)\frac{l_{min}}{c_d} \tag{13}$$

where $\propto$, ξ, l_{min} and c_d denotes time scaling factor, fraction of critical damping in the fundamental frequency mode, the shortest length of finite element and the dilatational wave speed, respectively. Dilatation wave speed can be represented as,

$$c_d \approx \sqrt{\frac{E}{\rho}} \tag{14}$$

Where E and ρ denotes Modulus of elasticity and material density, respectively.

3.2.2. Loading Rate

The purpose of this method is to reduce number of increments needed to complete the analysis using loading rate high as possible. However, high loading rate will create significant internal effects which leads to dynamic responses. Hence, loads should be applied as smooth as possible to maintain quasi-static condition. In the simulation, the smoothness of the applied loads or displacements was maintained through a fifth order polynomial function of time with first and second time derivatives equal to zero at the beginning and end of the time interval using the Abaqus/Explicit

keyword **Amplitude, Definition = Smooth Step*. Use of smooth step will ensure not to cause any accelerations enforced on the structure at the start and the end of a particular step.

It is important to identify smallest simulation time without any dynamic response throughout the entire time period. Only an estimation can be taken using fundamental natural mode of the whole structure since frequency and mode shapes will change during simulation period. Abaqus [43] recommends to use a time scale of 10 times the fundamental natural period of the structure as an initial estimate, which can be easily obtained by an eigenvalue analysis of the structure for its initial configuration. However, this will be a trial and error process using a sensitivity analysis to find out the suitable simulation time minimizing the dynamic behaviour of structure.

3.2.3. Numerical Damping

Numerical damping is used to damp out unwanted high oscillations chatter in the structure, to avoid sudden failure of elements due to large out of balance forces. Vibrations will lead to building up of high kinetic energy in the model. To dissipate build-up energy at high frequencies, numerical damping act as an efficient tool to maintain quasi-static behaviour. The amount of damping should be as small as required to prevent inaccurate results in simulation. Large values of ξ will result in an over-damped response that is not accurate, and decrease the stable time increment given by equation 12 (Δt decreases when ξ is increased), which leads to increased use of computational resources.

Bulk viscosity and viscous pressure, two methods available in Abaqus/Explicit for numerical damping are explained next.

Bulk viscosity involves in damping associated with volumetric straining in elements. There are two types of bulk viscosity, linear bulk viscosity and quadratic bulk viscosity. Linear bulk viscosity is used to damp out oscillations in all elements. Quadratic bulk viscosity smears the shock over several elements, but it is only applicable in solid continuum elements.

The linear and quadratic forms which generates a bulk viscosity pressure given as follows respectively,

Linear bulk viscosity $p_b = b_1 \rho c_d l_e \dot{\epsilon}_{vol}$ (15)

Quadratic bulk viscosity $p_b = \rho (b_2 l_e \dot{\epsilon}_{vol})^2$ (16)

Where b_1,b_2 are damping coefficient, l_e is an element characteristic length, and $\dot{\epsilon}_{vol}$ is the volumetric strain rate.

Second type of stabilization is achieved using viscous pressure loading. It is a very effective way to damp out dynamic effects to reach quasi-static equilibrium in a minimal number of increments. Viscous pressure introduces a velocity-dependent pressure on surface which is normal to shell elements. This pressure is given by,

$$p = -c_v v.n \tag{17}$$

Where c_v is the damping coefficient, v is the velocity and n is the normal vector.

The pressure waves crossing the free surface will be absorbed by viscous pressure load and there will not be any reflection of energy back to the interior of model. Unlike bulk viscosity, viscous damping will not affect stable time increment given in Equation 6. However, if the c_v value is high, it will overdamp the model and produce inaccurate results. Usually, c_v is set equal to very small percentage of ρC_d as given below,

$$\rho C_d = \rho \sqrt{\frac{E(1-v)}{\rho(1+v)(1-2v)}} \tag{18}$$

Where ρ, E, v are material density, Young's modulus and Poisson's ratio respectively.

3.2.4. Shear locking in fully integrated elements

First order fully integrated elements in finite element analysis software such as solid elements, Timoshenko beam elements, Mindlin plate elements can be overly stiff in bending applications. This numerical problem is called shear locking and it can create inaccurate results in simulation.

In an ideal scenario, an element will experience curved shape change under pure bending moment. Figure 3.2 illustrates a block of material with straight dotted lines on the surface and how the horizontal dotted lines and edges bend to curves while vertical dotted lines and edges remain straight under pure bending. The angle A, between horizontal and vertical dotted lines remain at 90 degrees as predicted by classical beam theory [44].

However, the edges of fully integrated first order elements are unable to bend to curves. Figure 3.3 shows the shape change of those elements under pure bending moment where all dotted lines are remaining straight while angle A is no longer 90 degrees. When the angle is not 90 degrees, an incorrect artificial shear stress is generated through shear deformation instead of bending deformation to maintain change in angle. This will result linear fully integrated elements to be locked or stiffed under the bending moment and show spurious results because of the locking.

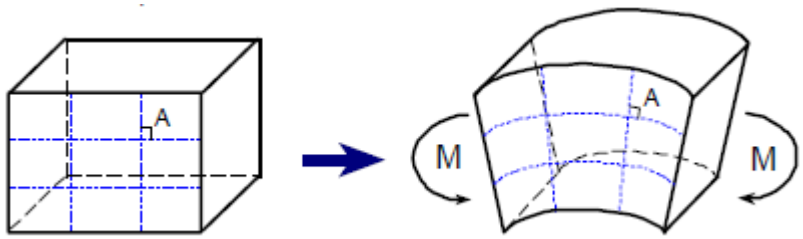

Figure 3.2: Shape change under pure bending moment in an ideal scenario

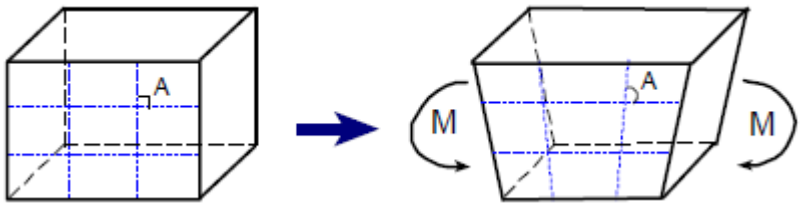

Figure 3.3: Shape change of fully integrated first order elements under pure bending moment

To overcome the above mentioned problems, fully integrated second order elements can be used. Edges of these type of elements have ability to bend to curves under a bending moment. It will correctly demonstrate real shape change of the

element and angle A will remain at 90 degrees as in an ideal situation as in Figure 3.4. No artificial shear stress is introduced and there will not be shear locking with 2nd order this type of elements.

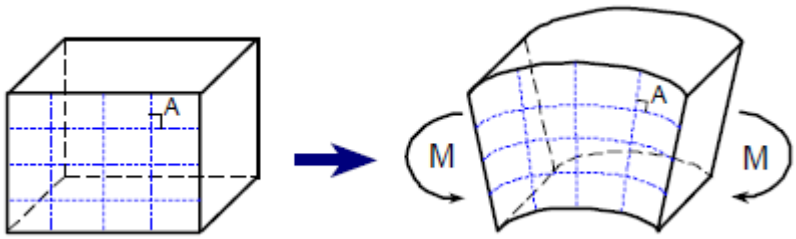

Figure 3.4: Shape change of fully integrated second order elements under pure bending moment

3.2.5. Energy Balance in quasi-static analysis

Results in Abaqus/Explicit solver is conditionally stable. Therefore, it is needed to carry out certain checks to ensure consistency and accuracy of the simulation.

The main method to verify robustness of a particular analysis is to investigate energy history. It helps to evaluate whether explicit simulation is providing an appropriate response. Mainly, the total energy stored and/or dissipated E_{tot} in the system should be equal to the work of external forces E_{wk}. According to Abaqus/Explicit energy balance equation can be written as,

$$E_{tot} = E_i + E_{vd} + E_{ke} - E_{wk} \quad (19)$$

Where, E_i is summation of internal energy consisting of elastic, inelastic strain energy and artificial strain energy due to hourglassing, E_{vd} is the viscous dissipation and E_{ke} is the kinetic energy.

In order to maintain quasi-static behaviour, inertia forces should be negligible. For that, kinetic energy in the system should be a very small fraction (1-5%) of its internal energy throughout the majority of simulation (Abaqus [43]). If the energy balance shows discrepancy, that indicates problems in the model with convergence

issues. When numerical instabilities are present, necessary changes should be done to maintain the quasi-static state. Artificial energy in structure has to be less than 1-2% of internal energy to ensure that simulation is free from excessive artificial effects like hour glassing and shear locking in Abaqus [43]. Therefore, it is necessary to check energy balance before coming to a conclusion from an explicit simulation output.

3.3. Simulation process of dual-matrix composite boom

The simulation sequence included three steps, folding, stabilization and deployment to follow the experiment discussed in Chapter 2. It is important to accurately capture initial stable folded configuration of boom to study quasi-static deployment behaviour. Simulation is started from unstressed fully deployed state as in Figure 3.6 (a). To fold the hinge to desired folded configuration, rotation is given at each end of the boom in opposite directions. But in practical scenario to prevent material damages in epoxy, boom is needed to be pinched or flattened first before folding. Hence, folding sequence is consisted with pinching, folding and pinch removing steps.

Following Ubamanyu et al. [41], first the boom was pinched using contact force applied through two rigid bodies to mimic the experimental procedure (see figure 3.6 (b)). Abaqus key word *General Contact* was used, which allows software to automatically detect potential contact surfaces including composite boom and rigid bodies (see figure 3.5) by specifying **Contact Inclusions, All Exterior*. Pinching force is simulated by giving an equal and opposite displacement to both rigid bodies over 0.3 s of step time.

After pinching is done, then the boom is rotated by specifying a 45^0 rotation to dummy node C over 5 s as in figure 3.6 (c). When fully folded configuration is achieved, two rigid bodies were removed over 0.3 s by specifying *Contact Extrusion,* to avoid any further constraints on the folded shape due to contact between boom and rigid bodies, figure 3.6 (d).

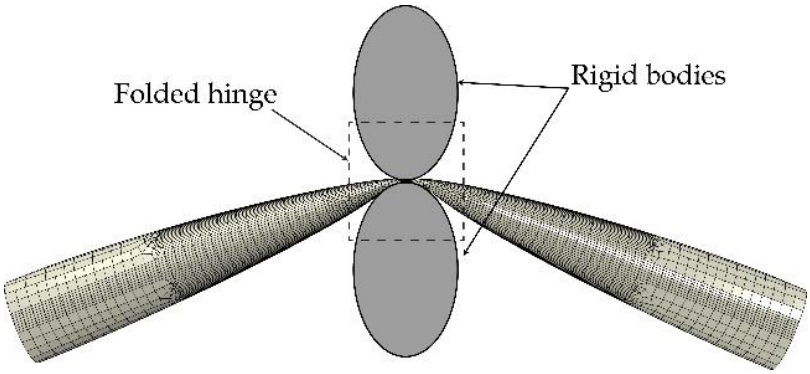

Figure 3.5: Folding using rigid cylinders

Once the folded configuration is achieved two ends were kept stationary for 1 s till it achieves the stable static configuration without changing any boundary condition. This will damp out the rise of kinetic energy due to sudden snapping after pinch removal. Finally after the stabilization, the boom was deployed over 10 s by rotating back dummy node C to 0^0 (see figure 3.6 (e)). All rotations were specified with a fifth order polynomial variation (*smooth step function) to avoid any accelerations at the beginning and end of each step to simulate quasi-static condition.

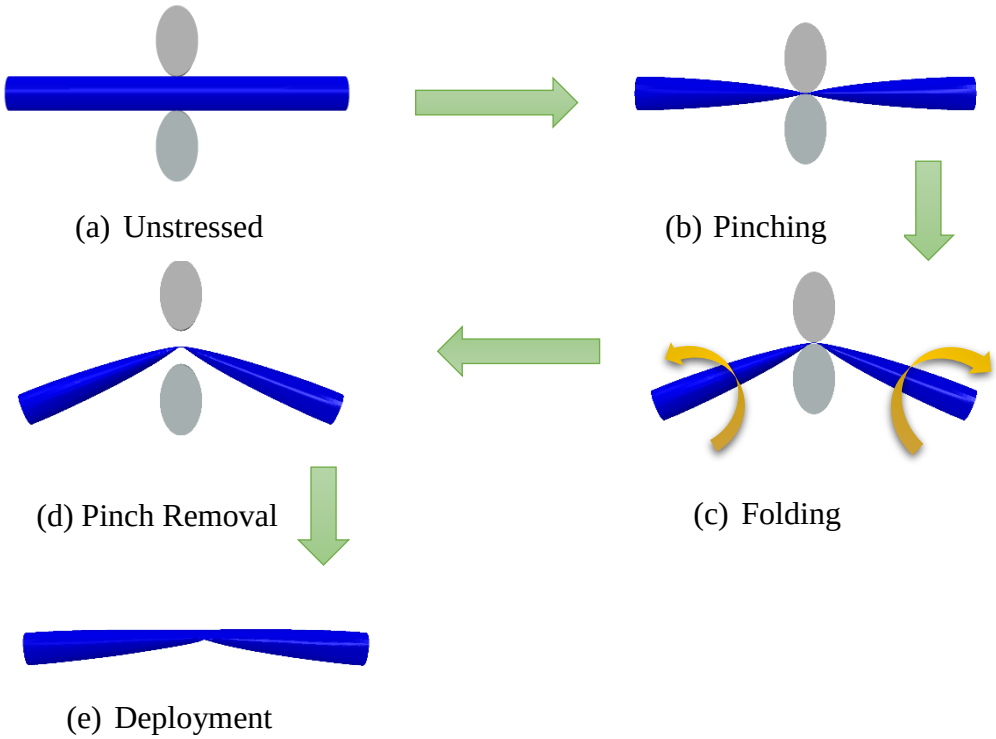

Figure 3.6: Folding simulation sequence

Linear bulk viscosity and viscous pressure were used to damp out high frequency oscillations [45]. Linear bulk viscosity factor was set to 0.1 and viscous pressure coefficient was set to 1.4528 $\times 10^{-3}$ kg $mm^{-1}s^{-1}$ to reduce kinetic energy and to achieve quasi-static equilibrium faster. Damping values were chosen such that kinetic energy is <1% of internal energy during deployment.

Figure 3.7 shows energy variation of simulation. Note that total energy remains zero throughout the simulation which confirms it is a stable solution. Slight rise of total energy at the end of the simulation is due to dynamic vibrations which is not considered in this study. Quasi-static behaviour is confirmed by keeping kinetic energy below 1% of strain energy. Sudden increase of kinetic energy corresponds to points of snapping which are dynamic events even when considering quasi-static experiments. Note that viscous dissipation rises mainly when high oscillations are to be damped.

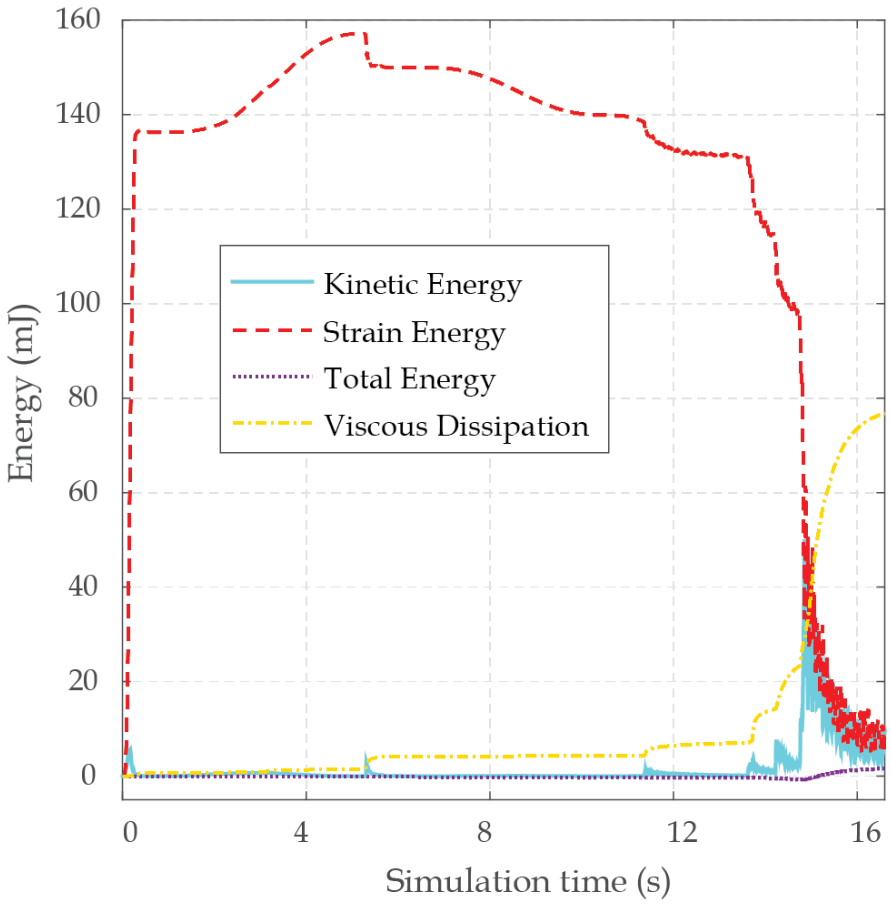

Figure 3.7: Energy variation of simulation

Results obtained through these simulations are presented in the following chapter and the key features are compared and discussed.

CHAPTER IV

4. Simulation Results

In this chapter characterization of the dual-matrix boom is carried out using the moment-rotation behaviour from the results extracted from simulation process mentioned under Chapter 3 is presented. Initially, thorough study was carried out to understand and to simulate fully folded hinge configuration. Next, change of transverse curvature with rotational angle was investigated to find out the effect of variable bending stiffness during the simulation process. Finally, comparison of moment-rotation response for quasi-static simulation with different bending stiffness is presented.

4.1. Folded Hinge

In simulation, when the boom with 100% of initial bending stiffness (100% D) in silicone region is pinched using rigid cylinders, it was observed that the boom forms a kink at the centre of the folded hinge soon after removing the rigid cylinders. Figure 4.1 shows two snapshots of boom hinge before the pinch removal and right after the pinch removal. Further examination of deformed cross section demonstrates that silicon hinge bends inward for its initial bending stiffness, which is an unrealistic folded configuration (see figure 4.2). As the stiff silicon hinge is reluctant to be flattened, tape springs are pushed back and the force generated by that tends to make the kink after the contact removal.

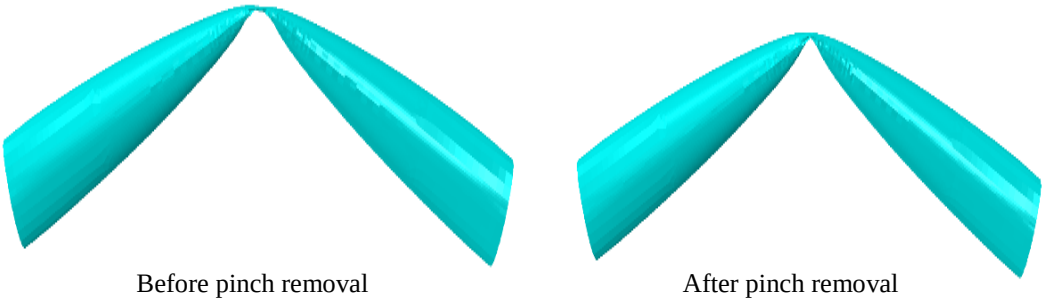

Before pinch removal After pinch removal

Figure 4.1: Kink at the centre of the fold after pinch removal

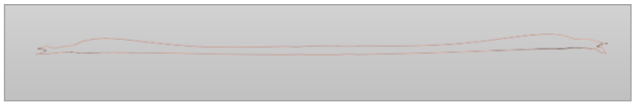

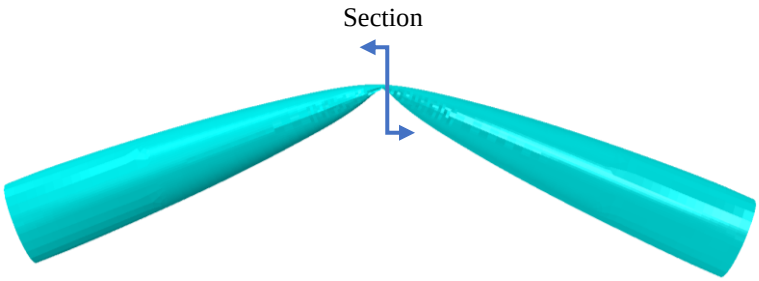

Figure 4.2: Fully deformed cross-section for 100% D

According to the kinetic energy plot, until the end of balancing step as shown in figure 4.3, there is clear energy rise at 5.3 s where the kink occurs with the geometric change after the pinch removal. This can affect quasi-static deployment behaviour of boom leading to oscillations in response due to vibrations. Balancing step of 1.0 s is used to damp out these high oscillations using viscous pressure load as mentioned in the previous chapter. However, viscous pressure was reduced to very small value before the start of deployment step to prevent the high damping effect on deployment behaviour.

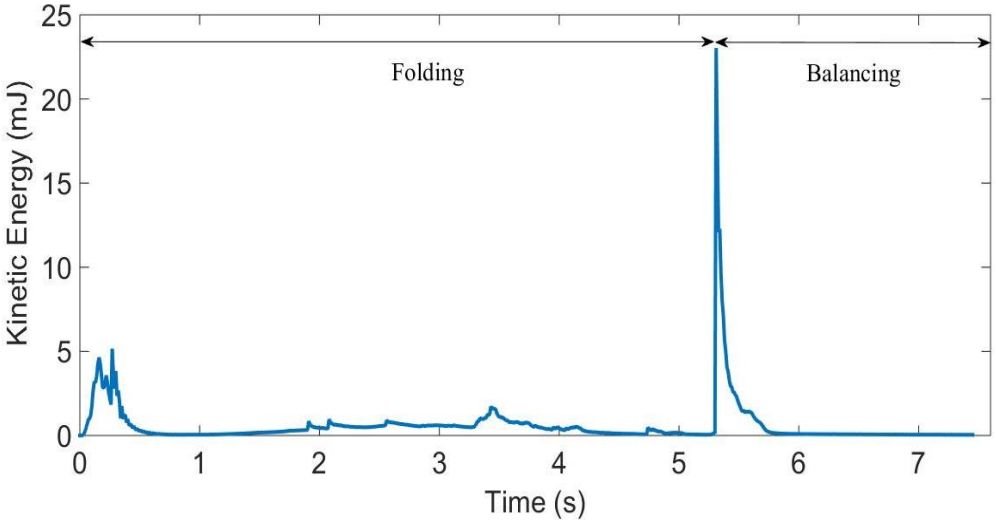

Figure 4.3: Kinetic energy plot until the end of balancing step

Following Sakovsky et al. [40] and Ubamanyu et al. [41] another simulation was run reducing bending stiffness (D matrix) in ABD matrix to 10% of its initial value. In figure 4.4, the cross section of folded hinge at centre for 10% D shows a more

realistic profile. This clearly confirms the reduction of bending stiffness in silicone matrix due to micro buckling in fibres under extreme curvatures, which is experimentally proven by Karl [26].

Figure 4.5 shows the variation of fully folded cross-section along the boom from centre (0 mm) to end after the stabilization using the balancing step. At the centre two tape-springs are tightly folded and towards the end of the boom, cross-section opens up rapidly showing an ovalized shape.

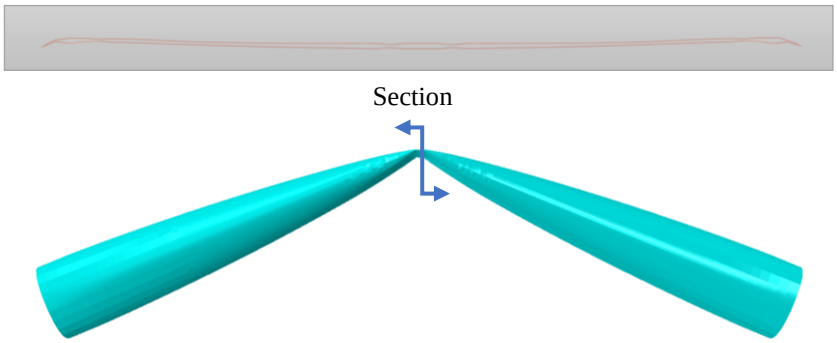

Figure 4.4: Fully deformed cross-section for 10% D

The understanding of transverse curvature is required to accurately predict deployment behaviour of dual-matrix composite boom with the variable bending stiffness. Figure 4.6 shows transverse curvature distribution for fully folded configuration for 10% D.

Figure 4.7 shows the maximum curvature variation of the hinge with respective deployment angle for simulations with 10% D and 100% D. Sudden change in curvature in both simulations corresponds to dynamic snap-back of the boom. Also, in both plots there is a small drop in curvature between $20^0 < \theta < 25^0$, where the other small peak moment can be expected due to snapping in outer tape-spring.

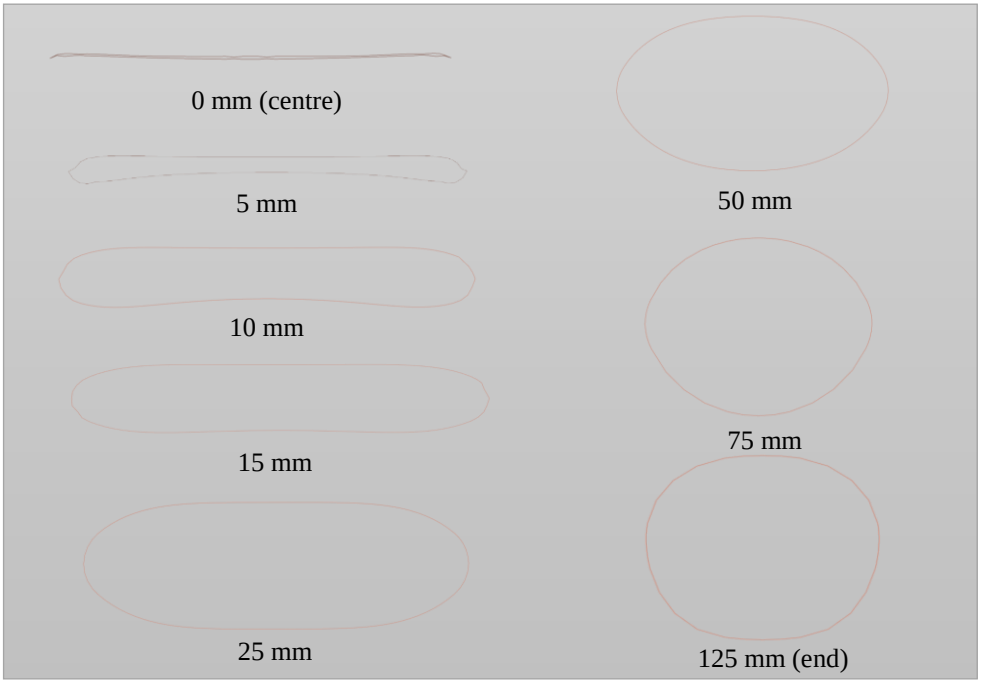

Figure 4.5: Variation of fully folded cross-section along the boom

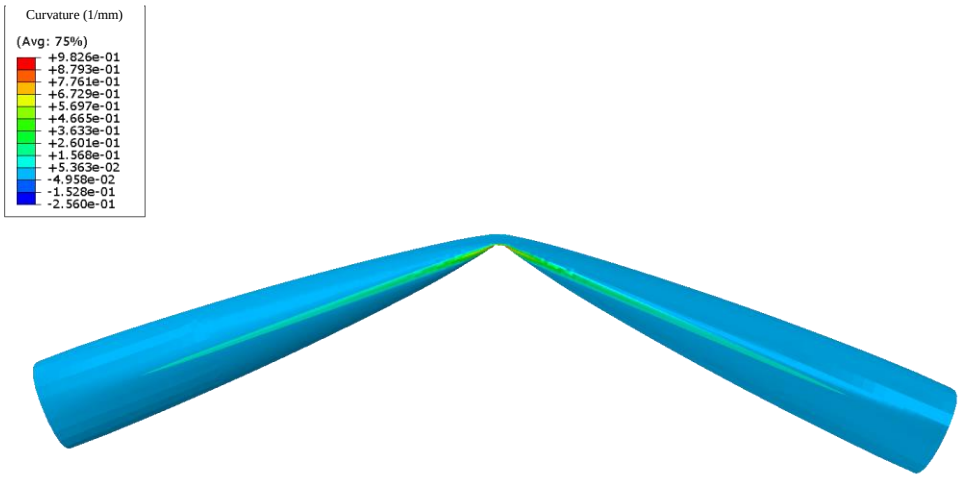

Figure 4.6: Transverse curvature distribution for fully folded boom

As expected stiffer 100% D simulation shows low curvatures compared to softer 10% D simulation. But there is a significant difference between 10% D and 100% D curvature values before the snapping and this implies that there is no sudden recovery back to initial bending stiffness of the reduced material bending stiffness due to extreme curvatures. Therefore, for a smooth deployment of dual-matrix hinge,

curvature and bending stiffness change should occur gradually. For an accurate characterization of dual-matrix boom, above mentioned curvature difference is needed to be captured and it was decided to study this effect using intermediate bending stiffness.

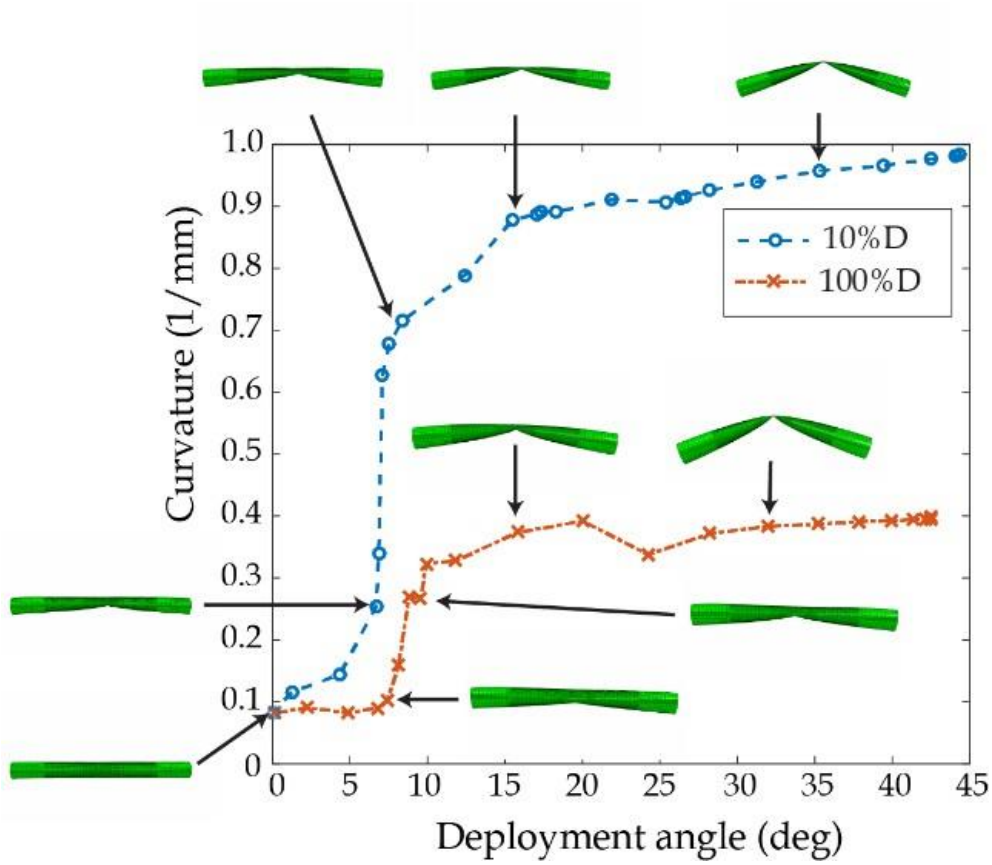

Figure 4.7: Variation of maximum curvature

Same simulation procedure mentioned in Chapter 3.3 was repeated with different bending stiffness coefficients (D matrix) for elastomer region to examine the bending behaviour. D sub-matrix of the complete ABD was changed to 50% and 70% of the original values apart from 10% and 100%.

4.2. Moment-Rotation Response of Quasi-Static Simulation

As mentioned in Chapter 2, moment-rotation response is used to characterize deployment behaviour of dual-matrix composite boom. Reaction moment corresponding to deployment angle was extracted from simulation output using dummy node to plot moment-angle response. Here, the deployment angle is defined as the angle between the two axes of straight portions of the boom.

Figure 4.8 compares the moment-rotation responses of simulations with 10%, 50%, 70% and 100% of bending stiffness coefficients for elastomer region against experimental results. Savitzky-Golay filter in MATLAB [46] was used to remove high frequency oscillations. Table 4.1 summarizes the main characteristics of all five cases.

Table 4.1-Comparison of boom characteristics

Model	Steady -state moment (Nmm)	Peak moment (Nmm)	Peak angle (deg)
10% D	33.3	484	5.7
50% D	76.6	599	6.4
70% D	85.4	706	8.1
100% D	129.9	833	8.2
Experiment	34.3	634	7.1

Note that all simulations and experimental results show a similar overall response and key characteristic values are in the same order of magnitude. Also as predicted for deployment of two tape-springs, it shows two separate peaks in graph. As one would expect, the moment corresponding to a given deployment angle rises with increasing bending stiffness in the silicone region. It can be observed that it is not realistic to reduce the bending stiffness to 10% D before $\theta=40^0$. 50% D and 70% D show a reasonable agreement with the experimental results from 12^0 to 30^0. However, 50% D shows significant deviation when it comes to peak-moment and corresponding angle.

Initial bending stiffness of the boom as well as peak-moment and peak-angle are better captured by the simulation with 100% D. It should be noted that the boom is not subjected to any localized deformations during deployment angles below the peak-angle and hence it is reasonable to use 100% of the bending stiffness at the initial stage. But still the predicted peak moment from simulation with 100% D is higher than the experimental peak moment. That is because folded hinge tends to self-deploy, which leads to lower peak moment in experiment. Further it should be noted that the apparatus used by Sakovsky et al. [40] is not sensitive to capture the absolute peak-moment.

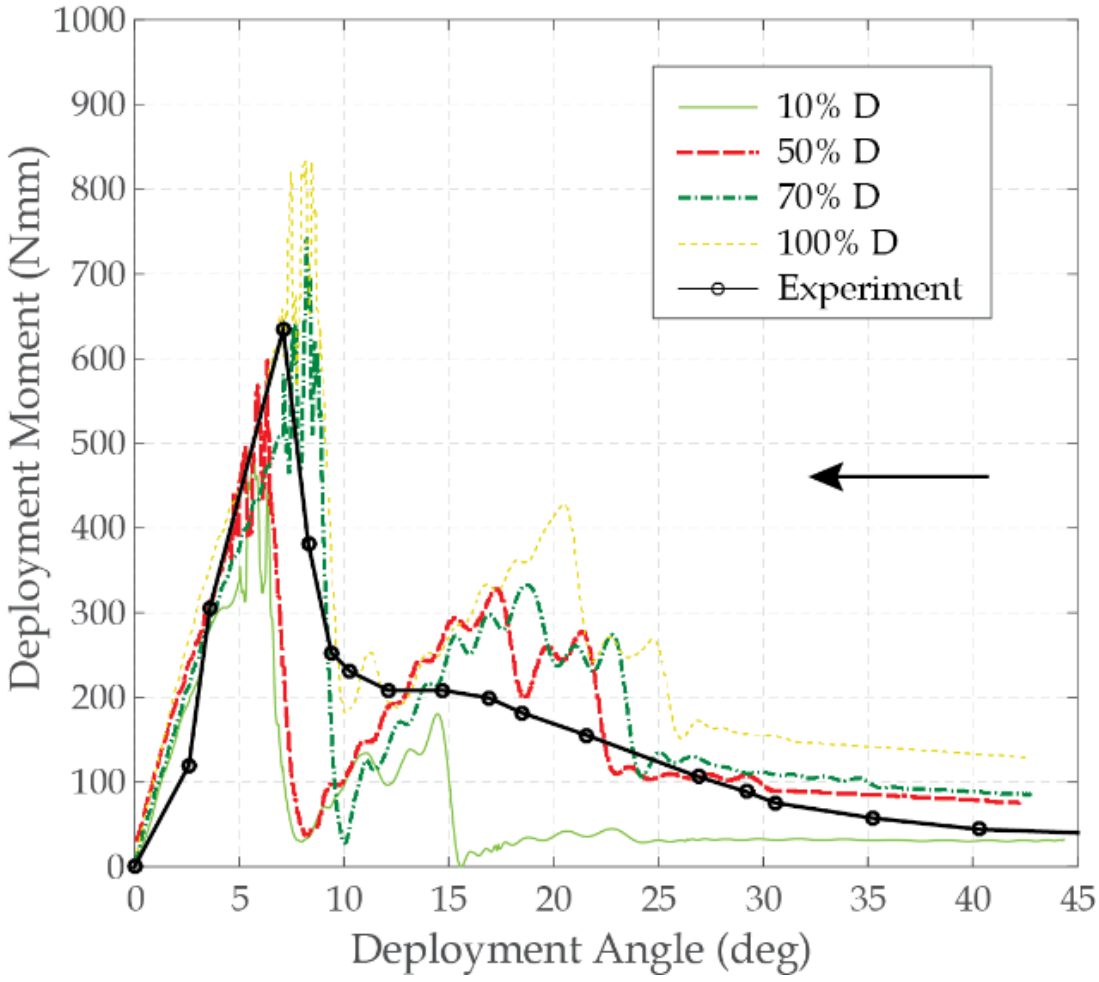

Figure 4.8: Comparison of moment rotation responses

CHAPTER V

5. Import Analysis

As described in Chapter 4, it is required to consider change of stiffness with degree of deformation in order for accurate prediction of deployment behaviour of hinges made of soft-elastomers. Since the features available in Abaqus [43] presently does not allow changing Section Definition during a simulation, possibility of transferring results of deformed structure to a new analysis and redefining Section Definition was investigated.

5.1. Introduction to Import Analysis

"*Import" feature in Abaqus allows transferring deformed mesh, associated material state and selected results to a new model where the material and section properties can be redefined. Results can be transferred from Abaqus/Standard to Abaqus/Explicit, Abaqus/Explicit to Abaqus/Standard, Abaqus/Standard to a new Abaqus/Standard model and Abaqus/Explicit to a new Abaqus/Explicit model as desired. When transferring model information and results from one analysis to another, user is allowed to decide on whether material state and stress state to be continued or not in the subsequent analysis. Table 5.1 shows a summary of import capabilities in Abaqus [43].

When using this import function, similar maintenance release of Abaqus/Standard and Abaqus/Explicit must be run on binary compatible computers. Furthermore transferring results from multiple analyses is not supported therefore transfer of results and model can be done only from one previous analysis.

Table 5.1 – Summary of import capabilities

Can be imported	Need to be re-specified	Cannot be imported
Material state	Boundary Conditions	Analytical rigid surfaces
Nodal Positions	Loads	Mesh-independent fasteners
Elements, element sets	Contact definitions	Connector elements
Nodes, node sets	Output requests	Dashpot and spring elements
Temperatures	Kinematic constraints	Mass and rotary inertia elements
Rebar layers	Nodal transformations	Infinite elements
	Amplitude definitions	Fluid elements

5.2. Finite element model

For the simulation of change in stiffness, sensitivity analysis was done using a plate which has geometry as shown in Figure 5.1, equal to the dimensions of silicon region in dual matrix composite boom described in Chapter 3. Finite element model of the plate was created and analysed using commercial finite element software package Abaqus/Explicit. In simulation plate is folded for 60^0 degrees and deployed back to the 0^0 to reach initial state.

The plate model consisted of 1000 S4R four node doubly curved shell elements with reduce integration and the minimum element size length was around 0.8 mm. Since the purpose of this sensitivity analysis was checking the capability of import analysis, reduced integration is used to reduce computational cost with a coarser mesh with an acceptable accuracy.

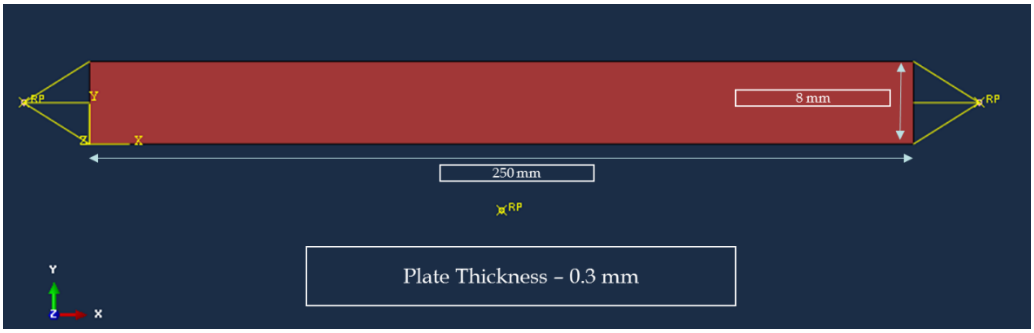

Figure 5.1: Geometry of the plate

Three sensitivity analyses were done with different material properties to check the capability of import analysis. In analysis 01 and 02 plate was assigned steel material properties and in analysis 03 plate was assigned ABD stiffness matrix (fibre-composites) with Silicone material properties. More details about the three analyses are explained further in next section.

The simulation is included folding, importing folded configuration with stress, strains and deployment. Folding and deployment of plate was done using a dummy node connected to two reference points with **Equation* constraint command in Abaqus, imposing similar boundary conditions which were used for dual matrix boom model in Chapter 3.1.

5.3. Analysis 01 – Transferring Results with the Constant Stiffness

The elastic properties of the isotropic material were defined as homogeneous using **Shell Section* keyword in Abaqus. The Young's modulus was 200 GPa, Poisson's Ratio 0.3 with Density of 7800 kg/m^3 respectively.

In the folding process 60^0 rotation was given to dummy node C using smooth step over 1s. After fully folded configuration was obtained, deformed mesh, associated material state and results were transferred to a new analysis without updating reference configuration using Abaqus keyword **Import, state=yes, update=no*. Here the state refers to the material state and update refers to the reference configuration. That will help to record translations, rotations and strains relative to initial position of the plate without resetting to zero again. When transferring initial condition to plate instances in the new model **predefined field*, Initial state was used to define deformed mesh and material state from last step of previous folded analysis. This was done at initial step since the creation of an initial field only available during the initial step. It should be noted that to verify import analysis, Young's modulus was kept as a constant during the analysis 01, to receive a solution without the effects due to change in stiffness. Figure 5.2 shows the stresses at the end of folded configuration and Figure 5.3 show folded configuration and stresses at the start after import analysis. Two figures show similar folded configuration with stresses and it implies that it is possible to transfer results from one analysis to another.

The deployment of updated new model was done by rotating node C back to 0^0 over 1 s with a smooth step definition. Figure 5.4 shows the final configuration of the plate after the deployment to the initial state. Stress shows value zero, similar as the original undeformed configuraiton. Furthermore Figure 5.5 and Figure 5.6 show moment variation over time during folding and deployment. At the end of the folding process moment is recorded as 50.04 Nmm. At the start of the analysis after the import analysis graph shows similar value of moment which is 50.04 Nmm and it confirm the correctness of importing stress and strains. After that, at the end of deployment process graph shows 0 Nmm as expected when plate comes to its initial position.

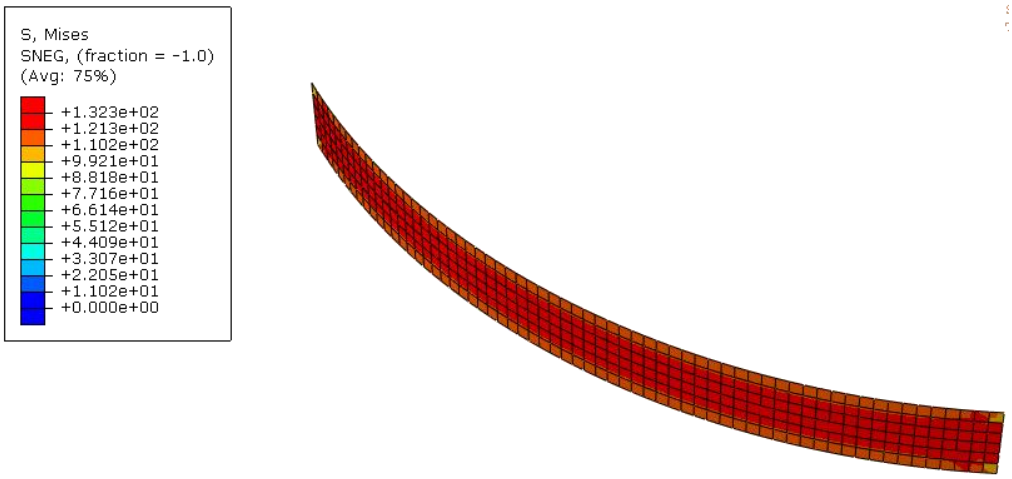

Figure 5.2: Stress distribution over the folded plate for analysis 01 at the end of folding step

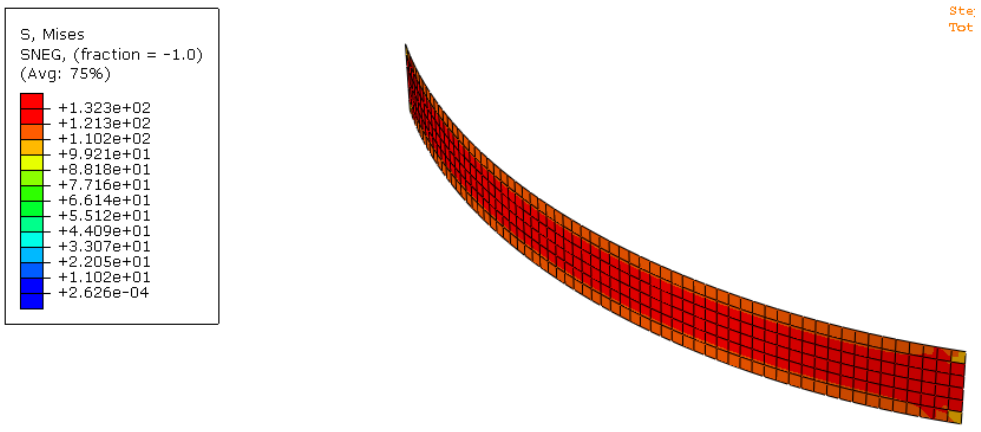

Figure 5.3: Stress distribution over the folded plate for analysis 01 soon after import analysis

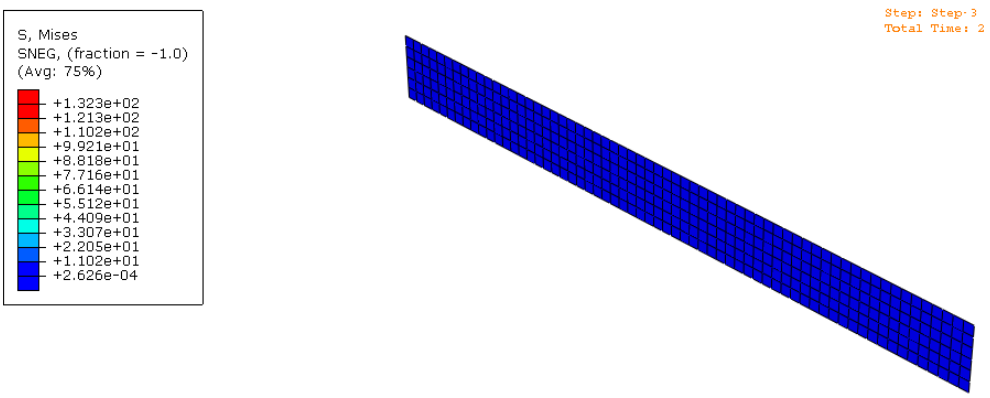

Figure 5.4: Stress variation of the plate for analysis 01 at the end of deployment using import analysis

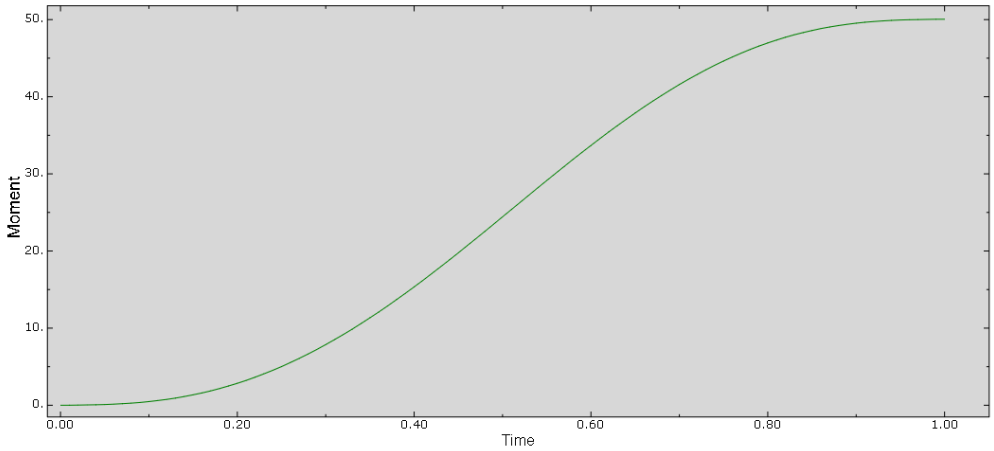

Figure 5.5: Folding moment for analysis 01

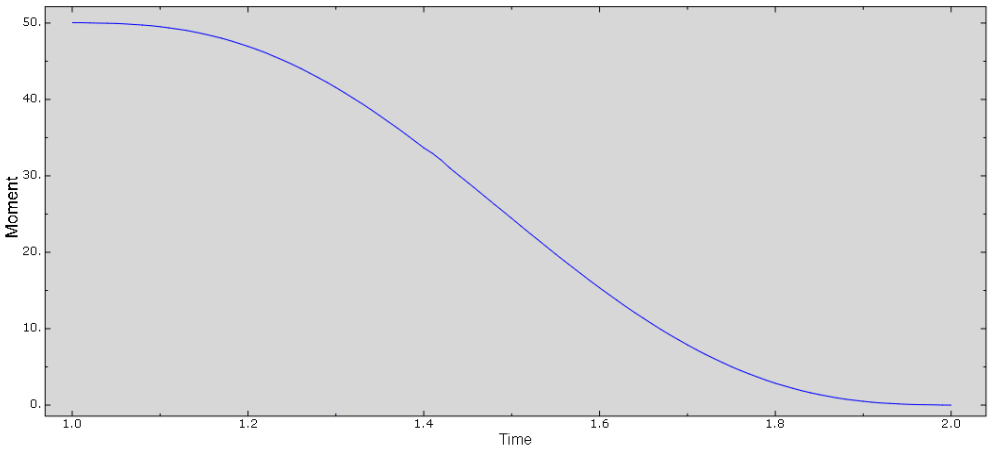

Figure 5.6: Deployment moment after using predefined fields for analysis 01

Also it is possible to import deformed mesh and the results from the intermediate step. But when the importing was done from an intermediate step to new Abaqus/Explicit analysis, the model may not be in static equilibrium. There will be inertia and damping dynamic forces at an intermediate step. If we neglect that and carried out the analysis there can be oscillations in the results and it is one of the main drawbacks in Abaqus import analysis. To study that affect, for a similar model described above was used. After folding, in new analysis deformed mesh, material state and other results were imported at 0.8 s using *predefined field* key word. After that step time was changed to 0.8 s for the deployment and simulation was done. As Figure 5.7 shows moment-time shows noise in the results as expected but which shouldn't be there.

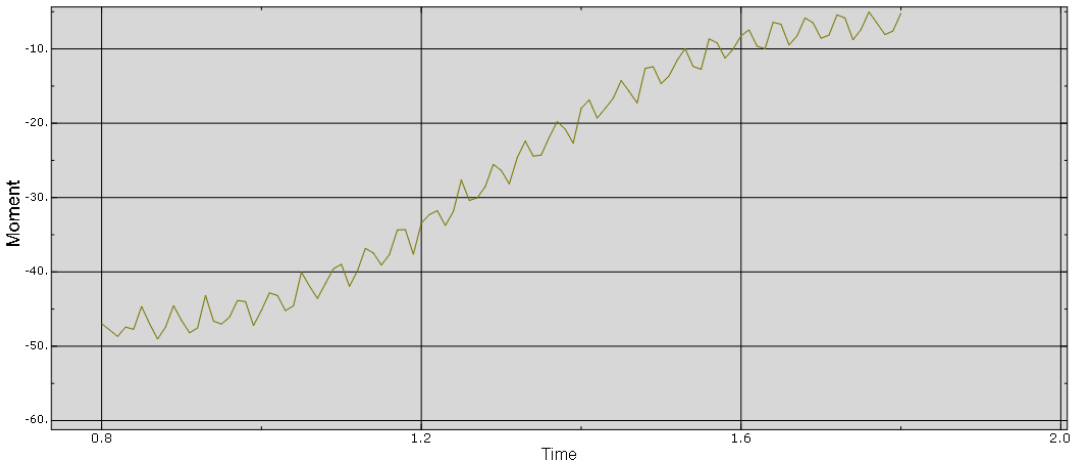

Figure 5.7: Deployment moment after using predefined fields at an intermediate time step (0.8 s)

Further a study was done to find a solution to remove these oscillations. It is proposed to reduce initial out of balance forces by introducing a smooth step at intermediate point when plate is folding, which will allow to achieve static equilibrium. Figure 5.8 shows the angle-time graph with a smoothing step at the intermediate time step. According to new moment-time graph shown in Figure 5.9, now there are no oscillations in the results. So it is very important to consider about the importing time step when doing the import analysis.

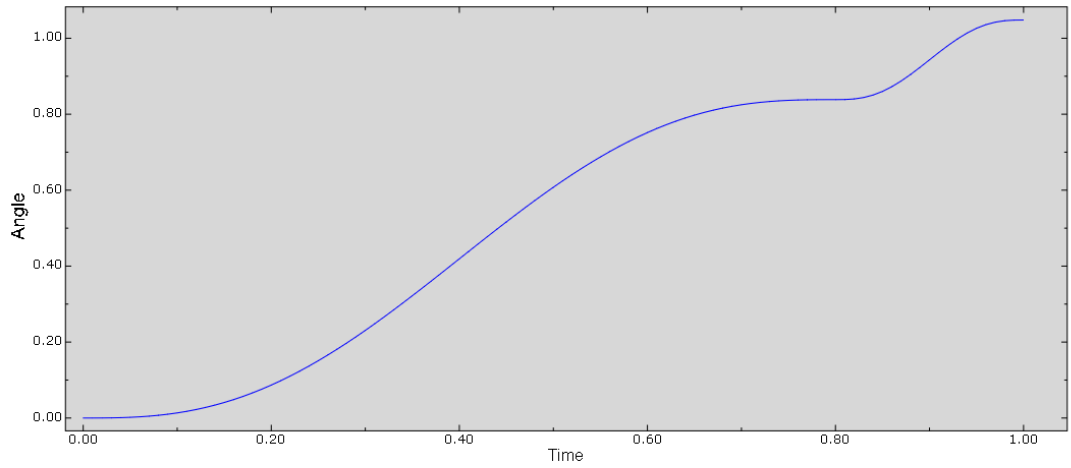

Figure 5.8: Folding angle with a smooth step at intermediate point (0.8 s)

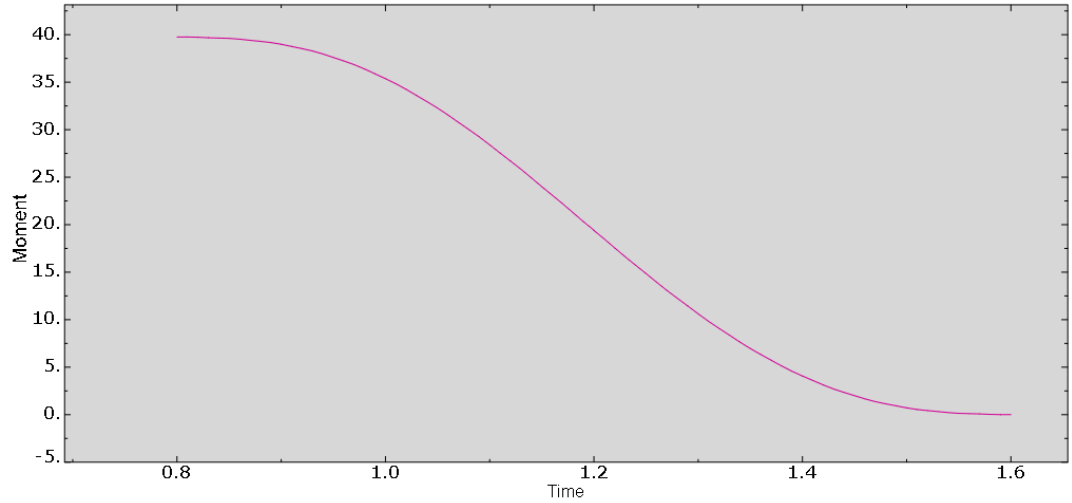

Figure 5.9: Deployment moment with a smooth step at intermediate point (0.8 s)

5.4. Analysis 02 – Transferring Results After Changing the Constant Stiffness

Analysis 02 is also done using similar properties and boundary conditions as mentioned in analysis 01. But in this analysis, after the result were transferred to new analysis using **predefined field* as previous, Young's modulus was changed to half of its initial value which is 100 GPa before the deployment. Then the deployment process is carried out rotating back dummy node C to 0^0 to achieve initial configuration.

At the end of the folding process moment of 50.04 Nmm is recorded as previous. But after that when the stiffness is changed, there is a clear variation in the moment-time plot as shown in Figure 5.10. There is a small drop in moment at the start point to which is 49.7 Nmm. Also the shape of curve is not smooth as analysis 01.

When the 0^0 is reached after the deployment, moment is not zero it has a value of 24.46 Nmm. This can be described using the residual stress remain in the plate as shown in Figure 5.11 after the deployment. Due to the sudden change in Young's modulus the residual stress is generated when plate comes to initial configuration and the moment is not set to zero. It is evident that the analysis can be used to change material properties during the simulation process and incorporate different Young's modulus. After this analysis, it is decided to check the capability to vary ABD stiffness matrix which is defined in shell general section using import analysis in Abaqus.

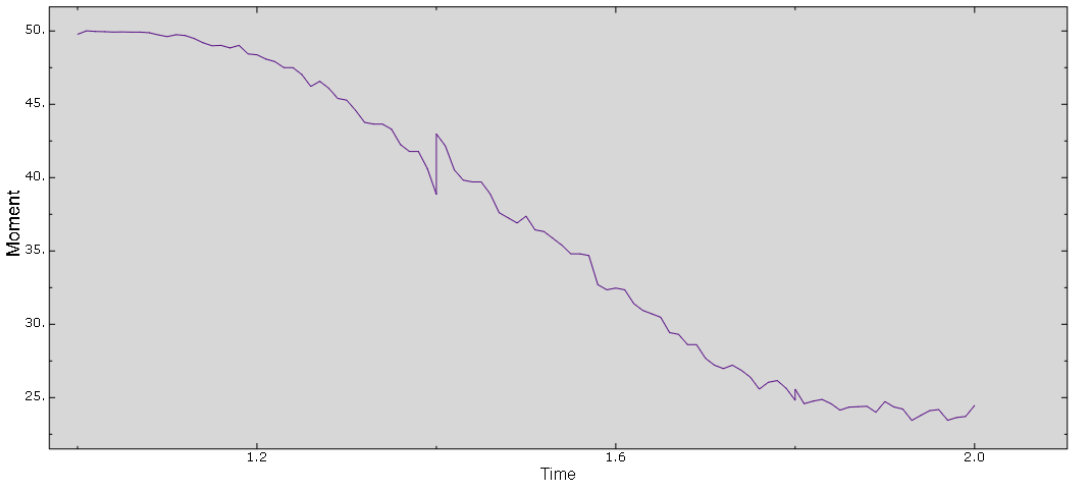

Figure 5.10: Deployment moment at the end of import analysis after using predefined fields at the end of the folding for analysis 02

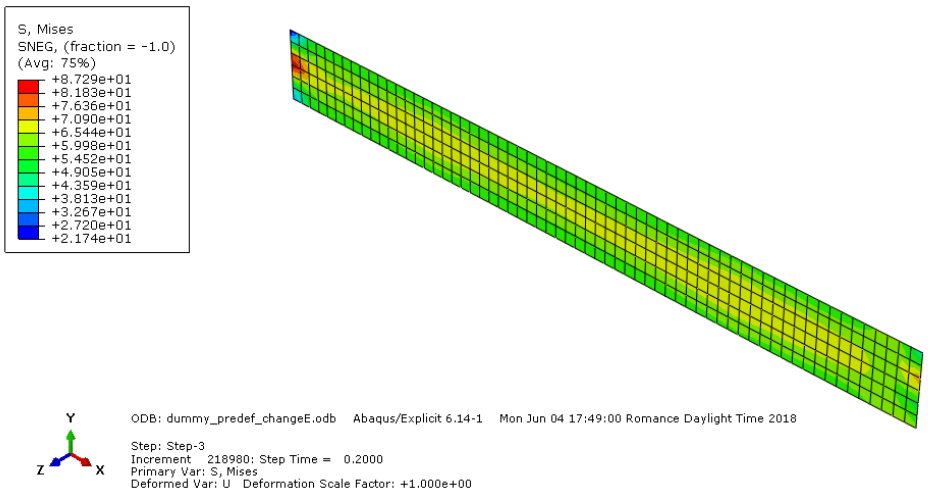

Figure 5.11: Stress for analysis 02 at the end of the import analysis

5.5. Analysis 03 – Transferring Results after Changing ABD Stiffness Matrix

In this analysis material properties of the plate are defined for 10%D of Silicon with ABD stiffness matrix as mentioned in equation 3 using **Shell General Section* keyword in Abaqus. First plate is folded as described in previous sections and after the folded configuration is achieved **predefined field* was used to transfer results of this analysis to a new analysis. In the new model ABD stiffness matrix is changed to 100%D to introduce variable stiffness matrix to study moment change with varying stiffness. Then the plate is folded back to initial unreformed shape by rotating back dummy node to 0^0.

When investigating the results it was visible that moment is not changing when the ABD matrix is changed during the simulation. After that thorough study was carried out to find out the reason and when investigating the Abaqus input file it is found that when **General Shell Stiffness* is used in Abaqus import analysis it is not behaving similar to *Shell Section*, which is used with Young's modulus. When the material property is defined with **General Shell Stiffness* and transfer results using import analysis, it is found that ABD stiffness of the new analysis has not been modified despite the new definition. Because of that even we change the ABD matrix values in new analysis, it is overwritten by the previous definition which is used to transfer material state with deformed mesh. Finally it can be concluded that Import analysis is not a suitable option to account variable bending stiffness in Silicone for ABD matrix using **General Shell Section*.

Another main drawback in Abaqus import analysis is when importing was done from an intermediate step to new Abaqus/Explicit analysis, the model is not in static equilibrium. There will be inertia and damping dynamic forces at an intermediate step. The initial out of balance forces were reduced by introducing a smooth step at intermediate point which will allow to achieve static equilibrium.

CHAPTER VI

6. User-Subroutine

This chapter presents simulations performed with user subroutine. Using user subroutine different material properties can be assigned during finite element analysis when the deployment angle change with the time. In this section codes are implemented to calculate membrane stresses in a solid and then the bending and membrane stresses in a shell using UMAT and UGEN user subroutines in the finite element software package Abaqus Implicit. Since it is only possible to define *Shell General Stiffness* using subroutine for implicit this solver is used.

6.1. Overview of Some User Subroutines

Customization of program for particular applications are allowed in Abaqus software using user subroutines. As an example user subroutine in Abaqus/Standard and user subroutine VUMAT in Abaqus/Explicit allow to add and change constitutive models in the program, while user subroutine like UEL, DLOAD in Abaqus/Standard allows to create user-defined elements and user-defined loading. Also in Abaqus/Standard, subroutines like CREEP is allowed to define time-dependent viscoplastic behaviour and Subroutines like DFLOW and FLOW is useful for consolidation analysis when defining non-uniform pore fluid velocity and non-uniform seepage coefficient. Furthermore there are subroutines like VDISP, VUAMP which are available in Abaqus/Explicit to define prescribed boundary conditions and to specify amplitudes. There are other subroutines also available in Abaqus [43] for both standard and explicit solver. Figure 6.1 shows the basic flow of data and actions in Abaqus/Standard analysis from start to end of a step. It demonstrates how the various subroutines are fitted at different steps of executing process.

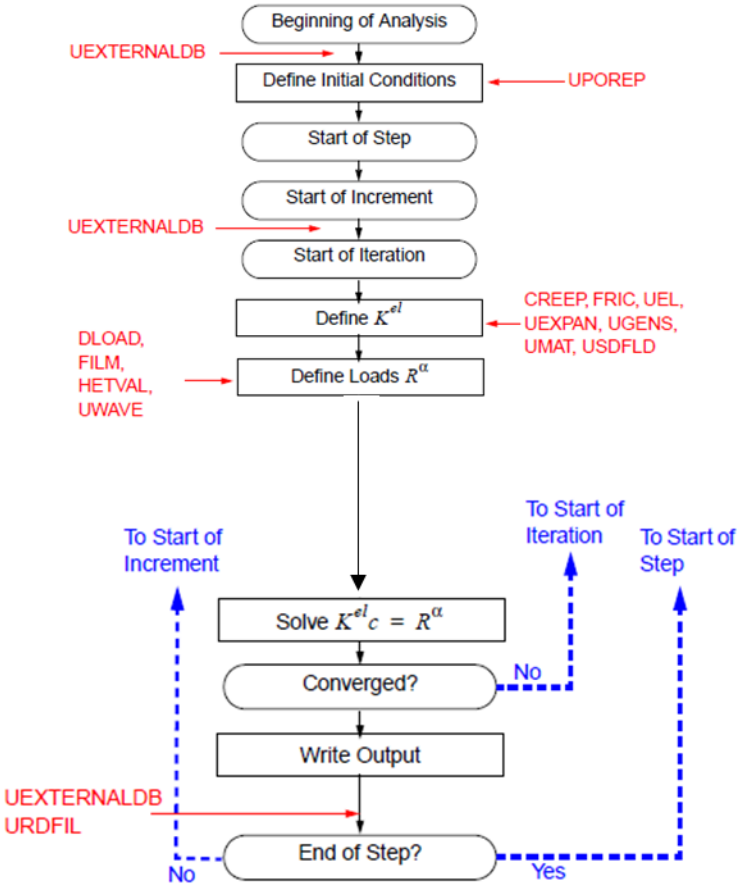

Figure 6.1: Global flow of Abaqus/Standard where User Subroutines fit into

6.2. Linking Abaqus with other software packages for subroutine

Simulia Abaqus is selective with FORTRAN and C++ compilers, their edition and linking environment. In this research Intel compiler with MS Visual Studio is used for linking. But it should be noted that every Intel Visual FORTRAN compiler and MS Visual Studio edition are not be able to linked and function properly with all Abaqus software editions. The following software packages are used for the user subroutine development, SIMULIA AbaqusTM 6.14, Microsoft Visual Studio 2012, Intel FORTRAN Composer XE 2013.

For the linking, computer's environment variables should be refreshed which are available in Advanced System Settings in computer. The infortvars.bat file in Intel Composer and the vevars64.bat file in the MS Visual Studio are located and directory is copied. Then the copied paths are pasted using add two lines in "Path" under the Environment Variables.

It is required to invoke Intel Parallel Studio and MS Visual Studio every time when Abaqus is running. For that Abaqus Command file and Abaqus CAE files are located and file targets are changed as described below respectively.

“C:\Program Files (x86)\Intel\Composer XE 2013\bin\ifortvars.bat" intel64 vs2012 & C:\Windows\SysWOW64\cmd.exe /k

"C:\Program Files (x86)\Intel\Composer XE 2013\bin\ifortvars.bat" intel64 vs2012 & C:\SIMULIA\Abaqus\Commands\abq6141.bat cae || pause

After the linking is done successfully, Abaqus command should visualize the screen as shown in figure 6.2. Figure 6.3 shows the computer process stepwise from start of Abaqus programme to compile and running the user subroutine.

Figure 6.2: Abaqus command after successful linking with FORTRAN compiler and MS Visual Studio

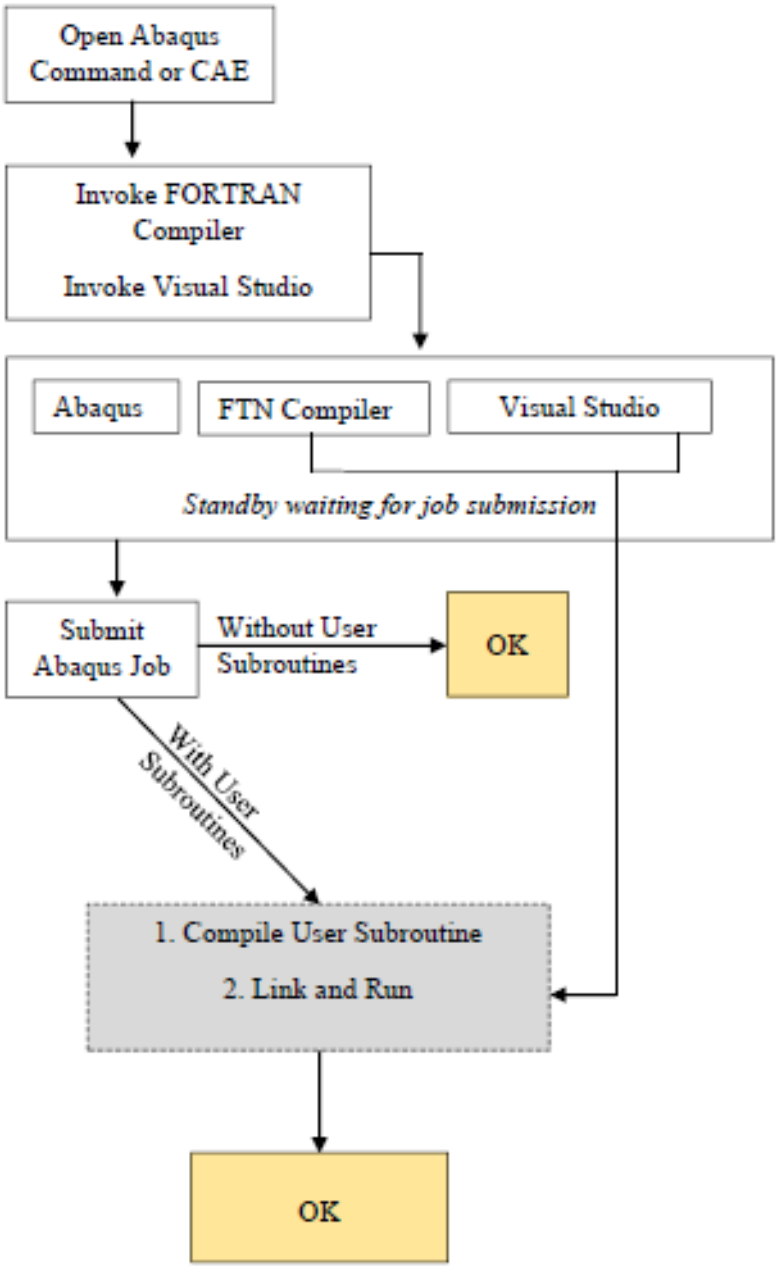

Figure 6.3: Flow chart describing the execution process in Abaqus with subroutine

6.3. UMAT

Abaqus has many calculation options in the software with the solver and it uses Jaumann stress derivative for implicit solver in 3D continuum elements. Nevertheless to define customize material behaviour UMAT (for implicit) subroutine, which is written in user-defined FORTRAN code can be implemented. This allows to define material with general constitutive equation for every integration point in the model and to change it with the requirement.

It is proposed to create a steel solid model with material properties mentioned in section 5.2.1. Tensile test is simulated with C3D8 elements with a UMAT subroutine to calculate membrane stresses using a code and another model is created with similar properties without the subroutine for the comparison.

In the FORTRAN code there is two way communication between the Abaqus software and the subroutine. In this process Abaqus main programme obtain necessary values from the subroutine to update them in UMAT subroutine and after the calculations in the code send them back to the model.

This whole process can be described further using headings of the subroutine as mentioned below. (Refer Appendix 1)

```
      SUBROUTINE UMAT (STRESS,STATEV,DDSDDE,SSE,SPD,SCD,
     1 RPL,DDSDDT,DRPLDE,DRPLDT,
     2 STRAN,DSTRAN,TIME,DTIME,TEMP,DTEMP,PREDEF,DPRED,CMNAME,
     3 NDI,NSHR,NTENS,NSTATV,PROPS,NPROPS,COORDS,DROT,PNEWDT,
     4 CELENT,DFGRD0,DFGRD1,NOEL,NPT,LAYER,KSPT,JSTEP,KINC)
C
      INCLUDE 'ABA_PARAM.INC'
C
      CHARACTER*80 CMNAME
      DIMENSION STRESS(NTENS),STATEV(NSTATV),
     1 DDSDDE(NTENS,NTENS),DDSDDT(NTENS),DRPLDE(NTENS),
     2 STRAN(NTENS),DSTRAN(NTENS),TIME(2),PREDEF(1),DPRED(1),
     3 PROPS(NPROPS),COORDS(3),DROT(3,3),DFGRD0(3,3),DFGRD1(3,3),
     4 JSTEP(4)
```

The heading must be included in every UMAT subroutine at the start. It described what are the values provided by Abaqus programme and what are the information that is needed to be send back to main programme by subroutine. Basically, the input data which is mentioned after the name for the user-defined UMAT material subroutine are the deformation variables such as deformation gradient, strain, strain increment, stress and state variables from the previous step. Also various information that might be used for some particular cases can be defined at the beginning, for example the step time and energy. The next group send the information back to main program after every increment in each step.

In the beginning of the increment stress array is passed as the stress tensor and the stress tensor must be updated at the end of the every increment. Stress vector is stored as this σ_{11}, σ_{22}, $\sigma_{33,}$ τ_{12}, $\tau_{13,}$ τ_{23}.

Then the Jacobian matrix of the constitutive model is defined with, $\frac{\Delta\sigma}{\Delta\varepsilon}$ where $\Delta\sigma$ is the stress increments and $\Delta\varepsilon$ (DSTRAN) is strain increments. The mechanical strains and the stress increments are passed to the subroutine at the beginning of the increment. Total strains are passed as an array of $\varepsilon_{1,}$ $\varepsilon_{2,}$ $\varepsilon_{3,}$ γ_{12}, γ_{13}, γ_{23}.

Figure 6.4 describes more information to understand how the Stress, Strain and strain increments arrays are made. In the graph i is the previous increment and the i+1 is the current increment. In the current increment Abaqus gives input variables to the subroutine from the previous increment. Stress (i), Strain (i) and stress increment is received for the subroutine at the beginning of the increment. FORTRAN code is calculating Stress (i+1) Strain (i+1), at the end of the current increment calculated values are sent to Abaqus programme.

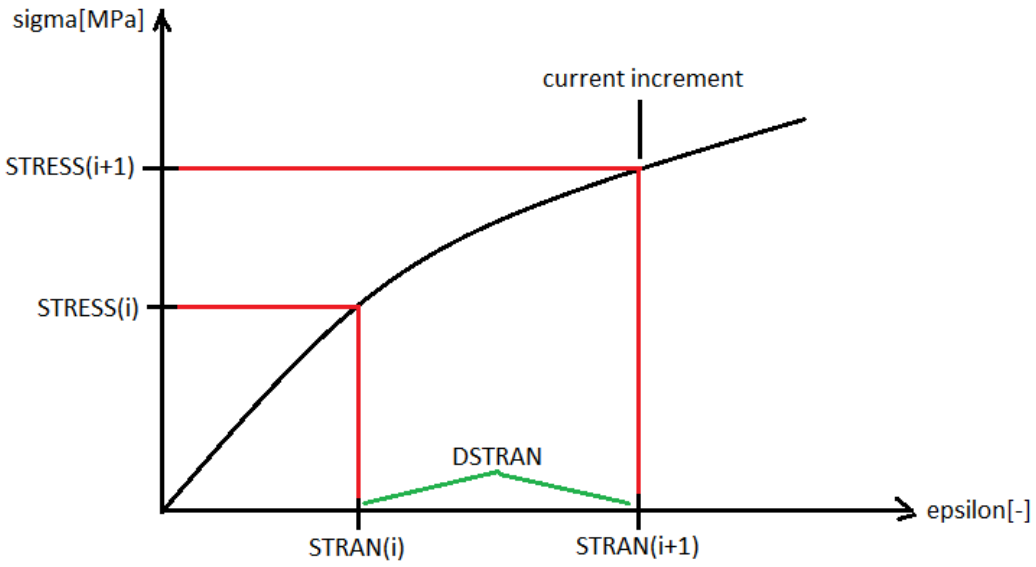

Figure 6.4: Change of stress and strain with the increment

In the Abaqus model, geometry with the mesh is created using in regular way defining the boundary conditions and applied tensile load. But the materials properties, Young's modulus and Poisson's ratio are not defined. The values of them are given as mechanical constants. After doing that Abaqus programme send these values to UMAT subroutine at every increment in an array named as PROPS array. At the end it was defined Abaqus to use user subroutine in every increment during numerical solving process of the model.

As mentioned above in the code UMAT subroutine receive the strains at the beginning of the increment with the mechanical constants. Using those constants stiffness matrix is given as a matrix. After that to calculate stress at each increment, the below equation is defined using the strain increment, stiffness matrix and the current stress with 2 loops, where I and J change from one to six.

$$STRESS(I) = STRESS(I) + DDSDDE(I,J)*DSTRAN(J)$$

At the end another model is created with similar geometry and properties by giving Young's modulus and Poisson's ratio without a subroutine in regular way and compared with the results of the subroutine. Both results (Figures 6.5 and 6.6) show the similar pattern which confirms the accuracy of the subroutine.

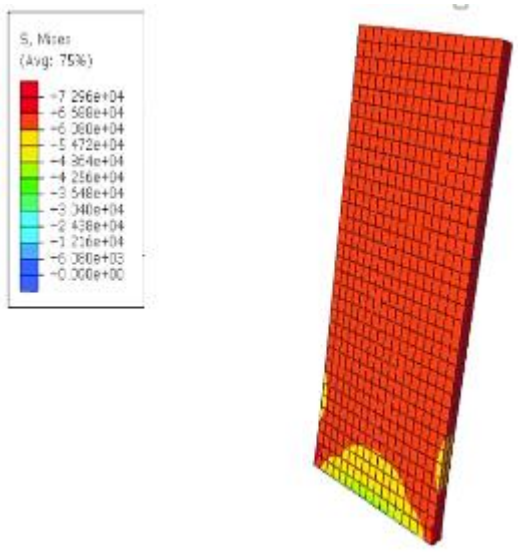

Figure 6.5: Final stress using subroutine

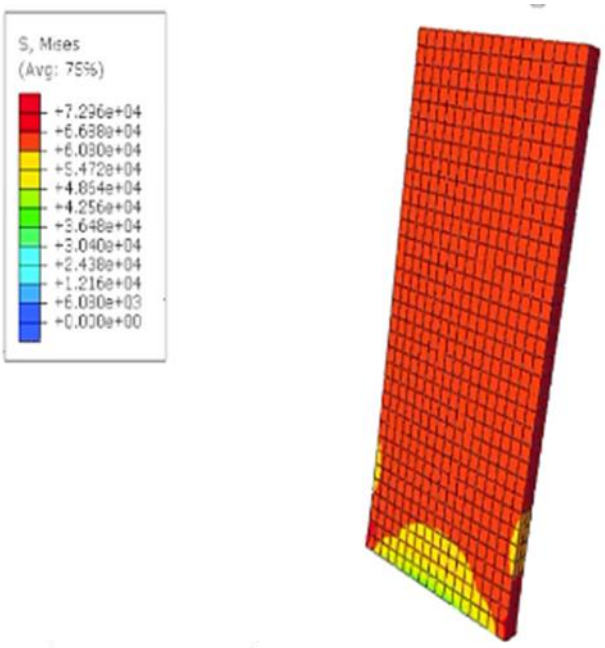

Figure 6.6: Final stress without using subroutine

6.4. UGEN

After simulating membrane stresses using subroutine next step is to simulate both membrane and bending stresses using the subroutine code. For every iteration in finite element analysis, the strain components of the shell elements are located in stiffness curves which is used to define the equivalent stiffness matrix, update moments and forces. In order to update mechanical behaviour of shell element in finite element model Abaqus UGENS subroutine can be used. That allows to calculate force on element after every load increment. Furthermore, it is possible to update state variables and other convergence parameters like Jacobian matrix using this subroutine.

In the following sections, input file and subroutine code preparation are explained stepwise.

6.4.1. Input File

The UGEN subroutine is developed to calculate membrane and bending stresses for a Silicone plate with S4 shell elements simulating pure bending with similar boundary conditions, material properties and other parameters as discussed in Section 5.2.3. The Abaqus input files need special preparation in-order to use the UGEN subroutine. The shell elements to assign ABD stiffness matrix and to follow the UGEN subroutine is defined using the **shell general section* abaqus command. Initial stiffness matrix of silicon is given defining symmetric part using 21 properties following equation 9 in Chapter 3. But if the stiffness matrix is unsymmetrical, each element should be defined using 36 properties.

*SHELL GENERAL SECTION, elset= name_of_element_set, USER, VARIABLES= number_state_var, PROPERTIES=21 (using symmetry of the matrix), density= 5.81e-07.

6.4.2. Subroutine File

The heading mentioned below should be used at the start of the UGEN subroutine. It consists with different parameters and values that are imported from Abaqus software and the information send back from subroutine to the Abaqus Programme as described in previous section.

```
  SUBROUTINE  UGENS (DDNDDE,FORCE,STATEV,SSE,SPD,PNEWDT,STRAN,
     1 DSTRAN,TSS,TIME,DTIME,TEMP,DTEMP,PREDEF,DPRED,CENAME,NDI,
     2 NSHR,NSECV,NSTATV,PROPS,JPROPS,NPROPS,NJPROP,COORDS,CELENT,
     3 THICK,DFGRD,CURV,BASIS,NOEL,NPT,KSTEP,KINC,NIT,LINPER)
C
      INCLUDE 'ABA_PARAM.INC'
C
      CHARACTER*80 CENAME
      DIMENSION DDNDDE(NSECV,NSECV),FORCE(NSECV),STATEV(NSTATV),
     1 STRAN(NSECV),DSTRAN(NSECV),TSS(2),TIME(2),PREDEF(*),
     2 DPRED(*),PROPS(*),JPROPS(*),COORDS(3),DFGRD(3,3),
     3 CURV(2,2),BASIS(3,3)
```

For every strain component in every element, Abaqus determines the strain at current increment ε_j, and next strain $\varepsilon_j + d\varepsilon_j$ and located in the corresponding strain array. In the subroutine code, total strain at current increment is calculated as below.

```
strainE(j)=STRAN(j) + DSTRAN(j)
```

Then the Jacobian stiffness matrix is updated using PROPS where the values are called from input files during code compiling and processing.

Finally the section forces are calculated using strain and stiffness arrays. For every finite element, every iteration, every strain increment a loop runs from (i = 1 to 6) and (j = 1 to 6). In the loop, index i loops among the force component, while j loops among the strain components. Bending and moment forces are given by,

```
FORCE(i) = FORCE(i)+DDNDDE(i,j)*strainE(j)
```

When the simulation is running it was stopped after few increments as in figure 6.7. It is found that convergence difficulties are observed when dramatic changes of mechanical properties are present between steps or among elements.

To improve the subroutine code decreasing maximum load step size, inducing the finite element package not to overshoot the next stiffness estimate and smoothing out sudden stiffness changes can be studied. Also the predefined strain points can be added to code input and then the stiffness curves can be interpolated using the pre-defined strains. The points can take arbitrary and same for the all stiffness. Number of

points can be decided on at what point it is needed to change the stiffness. Then the forces and moments can be calculated at strain points.

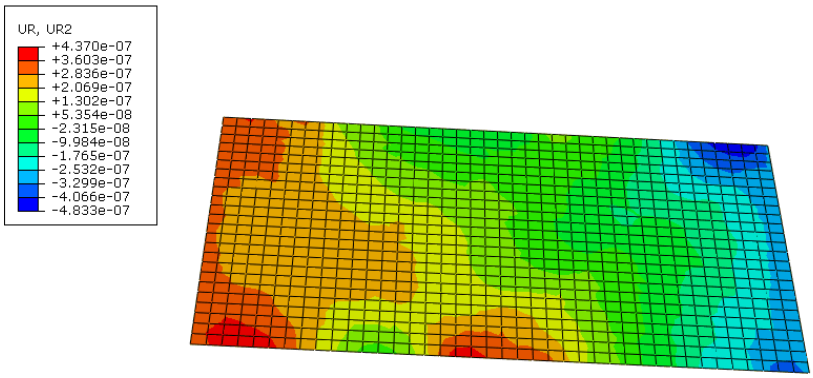

Figure 6.7: UGEN subroutine results up to termination

Furthermore stated variables can be added to the subroutine if it is required. The number of state variables for each element depends on the chosen integration procedure. At each integration point of the linear element, there are two state variables for the relative displacement (x- and y-direction) and the local stresses acting in the x- and y-direction. Furthermore, there is one value describing the current interaction state between the two surfaces for the purpose of stability analysis and position tracking during the numerical procedure. For a standard integration procedure with 3 integration points, this results in 15 (3x5) state variables for the linear element. As ABAQUS will not terminate the analysis if an insufficient number of state variables is provided for the chosen integration procedure, this user input error is checked within the subroutine.

CHAPTER VII

7. Conclusion

In this thesis, a detailed study of a dual-matrix composite boom made of weave glass fibre laminates is presented. A finite element simulation technique is used to predict quasi-static deployment behaviour of the composite boom.

Finite element model was developed using Abaqus/Explicit which is a commercially available finite element software package. Robustness of the explicit solver helped to reduce computational time for the simulation with a stable solution.

7.1. Important Findings and Discussion

It is shown that, bending stiffness of the elastomer region needs to be changed with degree of deformation of the hinge region for accurate prediction of bending behaviour of these type of dual-matrix composite booms. Variation of moment-rotation response with changing bending stiffness of the soft elastomer region has been compared against the experimental results available in literature. More reasonable agreement is shown capturing the peak moment and other areas in moment-rotation response, which were not captured in earlier researches. Also model predictions clearly show two distinct peaks in moment-rotation curve as predicted in analytical solution for two tape-spring boom, which was not captured during experiment.

However, for deployment angle from 8.2^0-12^0 reaction moment was not captured accurately. Therefore, rather than using a constant bending stiffness it is required to change the bending stiffness according to the curvature during simulation process.

The features available in finite element software does not allow changing the section definition during a simulation. Hence to simulate variable bending stiffness, import analysis was used to transfer deformed stress and strain state from a folded simulation and redefined section properties to corresponding reduction in bending stiffness. It is shown that, when there is a constant stiffness in the model it is possible to change material state and stress state during the analysis. Also analyses show that importance of keeping static equilibrium when importing from an intermediate step and the procedure to reduce inertia and damping dynamic forces. However, it is also shown

that when using ABD stiffness matrix, the stiffness matrix is not being modified despite the new definition with General Shell Section which is presently not fixed in Abaqus 6.14. Therefore it is not possible to use this method to simulated composite boom with a variable stiffness.

Next, attempts to simulate bending stiffness reduction with degree of deformation were performed through more complex User-defined Subroutines. Preliminary attempts on utilizing user-defined subroutine clearly indicates that the Shell Section definition can be updated to simulate the reduction in bending stiffness. Detail study showed how to make computer environment to link Abaqus software with other software packages for subroutine. In the process of creating user subroutine for shell section to simulate bending behaviour of composite, working subroutine is developed to calculate membrane stresses and compared with a model without the subroutine. It clearly shows exact results in comparison and the accuracy of the subroutine.

Proposed strategy with UGEN subroutine was studied to in cooperate variable bending stiffness for Shell General Section with membrane and bending stresses. The procedure to create the input file to be compatible with the UGEN subroutine for the ABD stiffness matrix is shown. However initial subroutine encountered convergence difficulties due to dramatic changes in mechanical properties between adjacent increments. It is identified that decreasing maximum load step size improves the subroutine. Smoothing out sudden stiffness changes and adding predefine strain points can be implemented.

7.2. Future Work

Presently the finite element programme does not have the capability to change stiffness with curvature during a simulation and it is intended to implement concurrent updating of section stiffness definition through user-defined sub-routine option.

Simulation technique for predicting deployment behaviour by incorporating variable bending stiffness in elastomer is still at the beginning. The next step is optimizing the sub-routine code for convergence. Then it is possible to define stiffness value according to the curvature. Ultimate goal is to develop simulation tool that can be used to update micro-scale response with the loads applied at macro-scale.

References

[1] H. Heidt, J. Puig-Suari, A. S. Moore, S. Nakasuka, and R. J. Twiggs, "CubeSat: A new Generation of Picosatellite for Education and Industry Low-Cost Space Experimentation," in *14th AIAA/USU Conference on Small Satellites*, 2000.

[2] P. Mallol and G. Tibert, "Deployment Modelling and Experimental Testing of a Bi-stable Composite Boom for Small Satellites," in *54th AIAA/ASME/ASCE/AHS/ASC Structures, Structural Dynamics, and Materials*, 2013.

[3] A. J. Cook and S. J. I. Walker, "Experimental research on tape spring supported space inflatable structures," *Acta Astronautica*, vol. 118, pp. 316–328, Jan. 2016.

[4] S. T. West, C. White, C. Celestino, S. Philpott, and M. Pankow, "Design and Testing of Deployable Carbon Fiber Booms for CubeSat Non-Gossamer Applications," in *56th AIAA/ASCE/AHS/ASC Structures, Structural Dynamics, and Materials Conference*, 2015.

[5] B. Osborne and C. Welch, "Short duration reduced gravity drop tower design and development," *JBIS - Journal of the British Interplanetary Society*, vol. 65, no. 2–3, pp. 71–76, 2012.

[6] T. Y. Liu, Q. P. Wu, B. Q. Sun, and F. T. Han, "Microgravity Level Measurement of the Beijing Drop Tower Using a Sensitive Accelerometer," *Scientific Reports*, vol. 6, pp. 1–9, 2016.

[7] C. R. Calladine, "The theory of thin shell structures 1888–1988," in *Proceedings of the Institution of Mechanical Engineers, Part A: Journal of Power and Energy*, vol. 202, no. 3, pp. 141–149, 1988.

[8] R. M. Jones, *Mechanics of Composite Materials*, 2nd edition. New York: Burnner-Routledge: Taylor and Fancis Group, 1998.

[9] M.I. Daniel and O. Ishai., *Engineering Mechanics of Composite Materials*, 2nd edition. Oxford University Press, 2005.

[10] R. F. Gibson, *Principles of Composite Material Mechanics*, 2nd edition, 2007.

[11] M. Sakovsky, "Design and Characterization of Dual-Matrix Composite Deployable Space Structures," PhD thesis, California Institute of Technology, 2018.

[12] O. Soykasap, "Micromechanical Models for Bending Behavior of Woven Composites," *Journal of Spacecraft and Rockets*, vol. 43, no. 5, pp. 1093–1100, 2006.

[13] L. S. Datashvili, H. Baier, and L. Schmidt, "Multi-scale Analysis of Structures Made of Triaxially Woven Fabric Composites with Stiff and Flexible Matrix Materials," in *52nd AIAA/ASME/ASCE/AHS/ASC Structures, Structural Dynamics and Materials Conference*, 2011.

[14] W. G. Jiang, "Implementation of domain superposition technique for the nonlinear analysis of composite materials," *Journal of Composite Materials*, vol. 47, no. 2, pp. 243–249, 2013.

[15] W. G. Jiang, S. R. Hallett, and M.R. Wisnom, "Development of Domain Superposition Technique for the Modelling of Woven Fabric Composites," *Mechanical Response of Composites. Computational Methods in Applied Sciences*, vol. 10, 2008.

[16] A. Kueh and S. Pellegrino, "ABD Matrix of Single-Ply Triaxial Weave Fabric Composites," in *48th AIAA/ASME/ASCE/AHS/ASC Structures, Structural Dynamics, and Materials Conference*, 2007.

[17] R. L. Karkkainen and B. V. Sankar, "A direct micromechanics method for analysis of failure initiation of plain weave textile composites," *Composites Science and Technology*, vol. 66, no. 1, pp. 137–150, 2006.

[18] J. Reveles, M. Lawton, V. Fraux, and V. Gurusamy, "The Development of a Low Mass Extendible Composite Boom for Small Satellite Applications," in *29th Annual AIAA/USU Conference on Small Satellites*, 2015.

[19] D. Lichodziejewski, B. Derbès, K. Slade, and T. Mann, "Vacuum deployment and testing of a 4-quadrant scalable inflatable rigidizable solar sail system," in

46th AIAA/ASME/ASCE/AHS/ASC Structures, Structural Dynamics & Materials Conference, Austin, Texas, 2005.

[20] H. Mao, G. P. Luigi, G. Michele, I. Nickolay, and T. Gunnar, "Deployment of Bistable Self-Deployable Tape Spring Booms Using a Gravity Offloading System," *Journal of Aerospace Engineering*, vol. 30, no. 4, p. 4017007, 2017.

[21] S. Seriani and P. Gallina, "A Storable Tubular Extendible Member (STEM) parallel robot: Modelization and evaluation," *Mechanism and Machine Theory*, vol. 90, pp. 95–107, 2015.

[22] J. C. H. Yee and S. Pellegrino, "Composite Tube Hinges," *Journal of Aerospace Engineering*, vol. 18, no. 4, pp. 224–231, 2005.

[23] D. Campbell, M. S. Lake and M. R. Scherbarth, "Elastic memory composite material: An enabling technology for future furable space structures," in *46th AIAA/ASME/ASCE/AHS/ASC Structures, Structural Dynamics, and Materials Conference, Austin, TX.*, 2005.

[24] R. Marissen and H. R. Brouwer, "The significance of fibre microbuckling for the flexural strength of a composite," *Composites Science and Technology*, vol. 59, no. 3, pp. 327–330, 1999.

[25] T. W. Murphey, T. Meink and M. M. Mikulas, "Some Micromechanics Considerations Of The Folding Of Rigidizable Composite Materials," in *42nd AIAA/ASME/ASCE/AHS/ASC Structures, Structural Dynamics and Materials Conference*, 2001.

[26] C. Karl, "Multifunctional dual-matrix composites for thin-walled deployable space structures," Master's thesis, Technische Universität München, 2015.

[27] H. M. Y. C. Mallikarachchi and S. Pellegrino, "Quasi-Static Folding and Deployment of Ultrathin Composite Tape-Spring Hinges," *Journal of Spacecraft and Rockets*, vol. 48, no. 1, pp. 187–198, 2011.

[28] H. M. Y. C. Mallikarachchi and S. Pellegrino, "Design of Ultrathin Composite Self-Deployable Booms," *Journal of Spacecraft and Rockets*, vol. 51, no. 6, pp. 1811–1821, 2014.

[29] H. M. Y. C. Mallikarachchi and S. Pellegrino, “Deployment Dynamics of Composite Booms with Integral Slotted Hinges,” in *AIAA/ASME/ASCE/AHS/ASC Structures, Structural Dynamics and Materials Conference*, 2014.

[30] P. A. Warren, B. J. Dobson, J. D. Hinkle, and M. Silver, “Experimental Characterization of Lightweight Strain Energy Deployment Hinges,” in *46th AIAA/ASME/ASCE/AHS/ASC Structures, Structural Dynamics & Materials Conference*, 2005.

[31] H. Yang, Z. Deng, R. Liu, Y. Wang, and H. Guo, “Optimizing the qusai-static folding and deploying of thin-walled tube flexure hinges with double slots,” *Chinese Journal of Mechanical Engineering*, vol. 27, no. 2, pp. 279–286, 2014.

[32] A. Stabile and S. Laurenzi, “Coiling dynamic analysis of thin-walled composite deployable boom,” *Composite Structures*, vol. 113, no. 1, pp. 429–436, 2014.

[33] C. Leclerc, L. Wilson, M. A. Bessa, and S. Pellegrino, “Characterization of ultra-thin composite triangular rollable and collapsible booms,” in *4th AIAA Spacecraft Structures Conference*, 2017.

[34] J. Block, M. Straubel, and M. Wiedemann, “Ultralight deployable booms for solar sails and other large gossamer structures in space,” *Acta Astronautica*, vol. 68, no. 7–8, pp. 984–992, 2011.

[35] D. Barbera and S. Laurenzi, “Nonlinear buckling and folding analysis of a storable tubular ultrathin boom for nanosatellites,” *Composite Structures*, vol. 132, pp. 226–238, 2015.

[36] Y. Hu, W. Chen, J. Gao, J. Hu, G. Fang, and F. Peng, “A study of flattening process of deployable composite thin-walled lenticular tubes under compression and tension,” *Composite Structures*, vol. 168, pp. 164–177, 2017.

[37] K. A. Seffen, Z. You, and S. Pellegrino, “Folding and deployment of curved tape springs,” *International Journal of Mechanical Sciences*, vol. 42, no. 10, pp. 2055–2073, 2000.

[38] K. A. Seffen and S. Pellegrino, “Deployment dynamics of tape springs,” in

Proceedings of the Royal Society A: Mathematical, Physical and Engineering Sciences, 1999.

[39] W. Szyszkowski, K. Fielden, and D. W. Johnson, "Self-locking satellite boom with flexure-mode joints," *Applied Mechanics Reviews*, vol. 50, pp. 225–231, 1997.

[40] M. Sakovsky, S. Pellegrino, and H. M. Y. C. Mallikarachchi, "Folding and Deployment of Closed Cross-Section Dual-Matrix Composite Booms," in *3rd AIAA Spacecraft Structures Conference*, 2016.

[41] K. Ubamanyu and H. M. Y. C. Mallikarachchi, "Simulation of Dual-Matrix Composite Boom," in *Proceedings of Annual Session of Society of Structural Engineers*, 2016.

[42] B. M. Ted Belytschko , Wing Kam Liu, *Nonlinear Finite Elements for Continua and Structures*, 1st edition. 2000.

[43] Abaqus, "Analysis User's Guide," Dassault Systemes Simulia Corp., Providence, Rhode Island, 2014.

[44] S. Gere, J. and Timoshenko, *Mechanics of Materials*, 4th edition. 1997.

[45] H. M. Y. C. Mallikarachchi, "Thin-walled composite deployable booms with tape-spring hinges," PhD thesis, University of Cambridge, 2011.

[46] MATLAB and Statistics Toolbox, "User's Guide (r2014b)." Mathworks Inc., 2014.

Appendix A

Removing high frequencies in response using Savitzky-Golay filter

```
%%% importing mom-rotation data
rot1new = radtodeg(rot1)-0.6342;    %%%angle radian to degrees
rot70new = radtodeg(rot70)-2.253;
rot100new = radtodeg(rot100)-2.459;
rot50new = radtodeg(rot50)-2.779;

%% %% smoothing
%%%%%10D 10D 10D
%
 k=0;
 tem1p1=sgolayfilt(mom1,9,777);
 tem2p1 = sgolayfilt(mom1,5,33);
 for k=1:9945
   if k<8100 | k>8350
    t1mom(k)=tem1p1(k);
   else
     t1mom(k)=tem2p1(k);
   end
 end

%% smoothing
%%%%%50D 50D 50D

 i=0;
 tem1p50=sgolayfilt(mom50,9,777);
 tem2p50 = sgolayfilt(mom50,5,33);
```

```
 for i=1:10006
   if i<6700 | i>7000
    t50mom(i)=tem1p50(i);
   else
     t50mom(i)=tem2p50(i);
   end
 end

%% %% %% smoothing
%%%%%70D 70D 70D

 j=0;
 tem1p70=sgolayfilt(mom70,9,777);
 tem2p70 = sgolayfilt(mom70,5,33);
 for j=1:10004
   if j<6400 | j>6680
    t70mom(j)=tem1p70(j);
   else
     t70mom(j)=tem2p70(j);
   end
 end
%% %% %% %% smoothing
%%%%%100D 100D 100D

n=0;
tem1p100=sgolayfilt(mom100,9,777);
tem2p100 = sgolayfilt(mom100,5,33);
for n=1:10004
```

```
   if n<6400 | n>6680
    t100mom(n)=tem1p100(n);
   else
     t100mom(n)=tem2p100(n);
   end
end
%% plot plot plot

%%plotting moment-rotation curve after smoothing.

plot(rot1new,t1mom,rot50new,t50mom,rot70new,t70mom,rot100new,t100mom)
```

Appendix B

Abaqus Subroutine Files

B.1 UMAT User Subroutine

```
      SUBROUTINE UMAT(STRESS,STATEV,DDSDDE,SSE,SPD,SCD,
     1 RPL,DDSDDT,DRPLDE,DRPLDT,
     2
STRAN,DSTRAN,TIME,DTIME,TEMP,DTEMP,PREDEF,DPRED,CMNAME,
     3 NDI,NSHR,NTENS,NSTATV,PROPS,NPROPS,COORDS,DROT,PNEWDT,
     4 CELENT,DFGRD0,DFGRD1,NOEL,NPT,LAYER,KSPT,JSTEP,KINC)
C
      INCLUDE 'ABA_PARAM.INC'
C
      CHARACTER*80 CMNAME
      DIMENSION STRESS(NTENS),STATEV(NSTATV),
     1 DDSDDE(NTENS,NTENS),DDSDDT(NTENS),DRPLDE(NTENS),
     2 STRAN(NTENS),DSTRAN(NTENS),TIME(2),PREDEF(1),DPRED(1),
     3 PROPS(NPROPS),COORDS(3),DROT(3,3),DFGRD0(3,3),DFGRD1(3,3),
     4 JSTEP(4)

C
      ELASTIC USER SUBROUTINE
       PARAMETER (ONE=1.0D0, TWO=2.0D0)
         E=PROPS(1)
         ACONNU=PROPS(2)
         ACONLAMBDA = E*ACONNU/(ONE+ANU)/(ONE-TWO*ACONNU)
         ACONMU = E/(ONE+ACONNU)/2
          DO I =1, NTENS
```

```
      DO J=1,NTENS
           DDSDDE(I,J) = 0.0D0
      ENDDO
     ENDDO

    DDSDDE(1,1)= (ACONLAMBDA+TWO*ACONMU)
    DDSDDE(2,2)= (ACONLAMBDA+TWO*ACONMU)
    DDSDDE(3,3)= (ACONLAMBDA+TWO*ACONMU)
    DDSDDE(4,4)= ACONMU
    DDSDDE(5,5)= ACONMU
    DDSDDE(6,6)= ACONMU
    DDSDDE(1,2)= ACONLAMBDA
    DDSDDE(1,3)= ACONLAMBDA
    DDSDDE(2,1)= ACONLAMBDA
    DDSDDE(2,3)= ACONLAMBDA
    DDSDDE(3,1)= ACONLAMBDA
    DDSDDE(3,2)= ACONLAMBDA

      DO I =1, NTENS
       DO J=1,NTENS
          STRESS(I) = STRESS(I)+ DDSDDE(I,J)*DSTRAN(J)
      ENDDO
     ENDDO

  RETURN
  END
```

B.2 UMAT User Subroutine

```
*USER SUBROUTINES
C**********************************************************************
****
C234567890123456789012345678901234567890123456789012345678901234567
89012
      SUBROUTINE
UGENS(DDNDDE,FORCE,STATEV,SSE,SPD,PNEWDT,STRAN,
     1
DSTRAN,TSS,TIME,DTIME,TEMP,DTEMP,PREDEF,DPRED,CENAME,NDI,
     2
NSHR,NSECV,NSTATV,PROPS,JPROPS,NPROPS,NJPROP,COORDS,CELENT,
     3 THICK,DFGRD,CURV,BASIS,NOEL,NPT,KSTEP,KINC,NIT,LINPER)


C
      INCLUDE 'ABA_PARAM.INC'
C
      CHARACTER*80 CENAME
      DIMENSION
DDNDDE(NSECV,NSECV),FORCE(NSECV),STATEV(NSTATV),
     1 STRAN(NSECV),DSTRAN(NSECV),TSS(2),TIME(2),PREDEF(*),
     2 DPRED(*),PROPS(*),JPROPS(*),COORDS(3),DFGRD(3,3),
     3 CURV(2,2),BASIS(3,3)


C     ELASTIC USER SUBROUTINE
      PARAMETER (ONE=1.0D0, TWO=2.0D0, THREE=3.0D0)



C-----update Jacobian (tangent stiffess)-----C
```

```
do i = 1, NSECV
 do j = 1, NSECV
DDNDDE(i,j)=0.0
 end do
end do

 DDNDDE(1,1)=PROPS(1)
 DDNDDE(1,2)=PROPS(2)
 DDNDDE(2,2)=PROPS(3)
 DDNDDE(1,3)=PROPS(4)
 DDNDDE(2,3)=PROPS(5)
 DDNDDE(3,3)=PROPS(6)
 DDNDDE(1,4)=PROPS(7)
 DDNDDE(2,4)=PROPS(8)
 DDNDDE(3,4)=PROPS(9)
 DDNDDE(4,4)=PROPS(10)
 DDNDDE(1,5)=PROPS(11)
 DDNDDE(2,5)=PROPS(12)
 DDNDDE(3,5)=PROPS(13)
 DDNDDE(4,5)=PROPS(14)
 DDNDDE(5,5)=PROPS(15)
 DDNDDE(1,6)=PROPS(16)
 DDNDDE(2,6)=PROPS(17)
 DDNDDE(3,6)=PROPS(18)
 DDNDDE(4,6)=PROPS(19)
 DDNDDE(5,6)=PROPS(20)
 DDNDDE(6,6)=PROPS(21)
```

```
      DDNDDE(2,1)=DDNDDE(1,2)
        DDNDDE(4,5)=DDNDDE(5,4)

C generalized section strains at the end of increment

      strainE(1)=STRAN(1) + DSTRAN(1)
      strainE(2)=STRAN(2) + DSTRAN(2)
      strainE(3)=STRAN(3) + DSTRAN(3)
      strainE(4)=STRAN(4) + DSTRAN(4)
      strainE(5)=STRAN(5) + DSTRAN(5)
      strainE(6)=STRAN(6) + DSTRAN(6)


      do i = 1, NSECV
       do j = 1, NSECV
       FORCE(i) = FORCE(i)+DDNDDE(i,j)*strainE(j)
       end do
      end do

    RETURN
    END
```